Discontinuous Galerkin methods for non-isothermal Darcy-Forchheimer flows

Numerical Analysis for PDEs

Students: ANDENA T. - BOTTACINI G. - BRUNELLI F.
Supervisors: BONETTI S. - BOTTI M.

Report for the project of the course of
Numerical analysis for PDEs

Mathematical engineering
Politecnico di Milano
Italy
September 18, 2023

Contents

Introduction

The purpose of this project is to implement discontinuous Galerkin methods for the numerical simulation of non-isothermal flows in porous media. The interest in this topic is motivated by its practical applications, such as the optimization in the production of geothermal energy and geological CO2 storage activities; the aim is to exploit all the flexibility given by the discontinuous discretization in order to treat more general problems, with more general data and domains. First, we introduce the mathematical equations that characterize the physical phenomena of interest: in order to model the flow of an incompressible fluid through a fractured media we exploit the Darcy-Forchheimer equation, which links pressure loss caused by friction across the medium with respect to the velocity of the flow. This choice is justified by the fact that the Darcy's law loses sense for high-velocity fluids, in which we are interested instead, and by the geometry of the fractured media that is indeed very irregular. Moreover, since we want to take into account the influence of the variation of temperature, we coupled the first empirical equation with an advection-diffusion equation that describe the evolution of the temperature of the flow. It is important to remark that when a fluid is subject to a temperature change, its physical properties such as density and viscosity may change; this yeilds to a coupling between the equations where one influences the other and viceversa. All these behaviours are express by the following set of equations:

$$\nu(\theta)\boldsymbol{u} + \beta|\boldsymbol{u}|\boldsymbol{u} + \nabla p = \boldsymbol{f} \ \text{ in } \ \Omega, \tag{1.1}$$

$$\operatorname{div} \boldsymbol{u} = 0 \ \text{ in } \ \Omega, \tag{1.2}$$

$$-\kappa\Delta\theta + (\boldsymbol{u}\cdot\nabla)\theta = g \ \text{ in } \ \Omega, \tag{1.3}$$

where Ω is an open bounded set in $\mathbb{R}^d$ (d = 2,3) with a Lipschitz-continuous boundary $\partial\Omega$ and an unitary outer norm $\boldsymbol{n}$. By $|\cdot|$ we mean the Euclidean vector norm, namely $|u|^2 := u \cdot u$. The unknowns that describe the physical quantities of interest are the velocity field $\boldsymbol{u} : \Omega \to \mathbb{R}^d$, the pressure scalar field $p : \Omega \to \mathbb{R}$ and the temperature scalar field $\theta : \Omega \to \mathbb{R}$. On the other hand the data of the problem are the external body force that act on the fluid (per unit volume) $\boldsymbol{f} : \Omega \to \mathbb{R}^d$ and the external heat source (or sink) $g : \Omega \to \mathbb{R}$. We also introduce the thermal conductivity $\kappa > 0$, the nonlinear viscosity of the fluid $\nu(\theta) > 0$ that depend on the temperature θ and finally the Forchheimer coefficient β which describes the porosity of the medium: it is the ratio of pressure drop caused by fluid–solid interactions to that by viscous and inertia resistances. If β was null then (1.1) it would be reduced to the Darcy's equation. It is worthy to note that the couplings between (1.1) and (1.3) are express through the convective term $(\boldsymbol{u}\cdot\nabla)\theta$, hence the velocity of the flow affects the direction of the heat, and the term $\nu(\theta)\boldsymbol{u}$, namely the kinematic viscosity of the fluid change accordingly with the temperature. In order to obtain a well posed problem we can choose between two possible boundary conditions:

$$\begin{gathered} \boldsymbol{u}\cdot\boldsymbol{n} \ \text{ on } \ \partial\Omega \quad \text{and} \quad \theta = \theta_0 \ \text{ on } \ \partial\Omega \\ \text{or} \\ p = p_D \ \text{ on } \ \partial\Omega \quad \text{and} \quad \theta = \theta_0 \ \text{ on } \ \partial\Omega \end{gathered} \tag{1.4}$$

the first choice is made by a constrain on the normal component of the velocity, and a given temperature distribution $\theta_0 : \Omega \to \mathbb{R}$, moreover, in this case one has to enforce

$$\int_\Omega p \, dx = 0$$

in order to close the problem. Instead the second case consists in two Dirichlet conditions for both pressure and temperature. The system (1.1),...,(1.4) and its nomenclature are borrowed from [1] where an unique solvability of the problem is proved. In [1] is also presented a numerical investigation of a continuous formulation approximated with conforming finite element scheme. The remaining parts of this report are structured as follow: in the first chapter we deal with the analytical and numerical analysis of the linear decoupled version of the system (1.1),...,(1.4), namely we describe separately the Darcy system and the advection-diffusion equation and their own formulations. Right after, we reintroduce the convective term $(\boldsymbol{u}\cdot\nabla)\theta$ in (1.3) and we solve

in cascata the two systems. The third chapter focus on how to treat the non linearity in (1.1) and how to solve the equation exploiting some fixed point techniques. Finally, in the last chapter we deal with the complete problem, reporting the complete analysis and the numerical investigation.

Notation	Quantity	Unit
ν	viscosity of the fluid	$\mathrm{Kg}/(\mathrm{m\,s})$
β	Forchheimer coefficient	Kg/m^2
κ	thermal conductivity	$\mathrm{W}/(\mathrm{m\,K})$

Table 1.1: Physical parameters appearing in (1.1)...(1.4)

Decoupled Problems

In this section we presented the analysis of two different systems, with the purpose of achieving some preliminary information about the weak formulations of the problems and their numerical behaviours. Starting from the original problem we obtained two new systems by erasing the non-linearity and neglecting all the coupling terms. Hence in (1.1) we set $\beta = 0$ and we considered the kinematic viscosity independent of the temperature, $\nu(\theta) = \nu$, in this way we got the classic linear Darcy problem:

$$\begin{cases} \nu \boldsymbol{u} + \nabla p = \boldsymbol{f} \ \text{ in } \ \Omega, \\ \operatorname{div} \boldsymbol{u} = 0 \ \text{ in } \ \Omega, \\ p = p_D \ \text{ on } \ \partial\Omega \end{cases} \tag{2.1}$$

Moreover, by considering $\boldsymbol{u}$ as an arbitrary convective velocity (for the sake of notation we will call it $\boldsymbol{u}$ even if it is not the solution of the first problem) we obtained the following advection-diffusion system in non-conservative form:

$$\begin{cases} -\kappa \Delta \theta + \boldsymbol{u} \cdot \nabla \theta = g \ \text{ in } \ \Omega, \\ \theta = \theta_0 \ \text{ on } \ \partial\Omega \end{cases} \tag{2.2}$$

Before starting with the analysis of the problems we set the notations that we will use until the end of the report, moreover, in the next section we introduced some useful concepts for building a discrete formulation.

2.1 Notation, preliminaries and discrete setting

In this section we introduced the setting for writing systems (2.1) and (2.2) in the variational form. Later, we also introduced the fundamentals for modeling the problems via dG methods. We relied on the standard notation, thus we defined the *first order Sobolev space* in dimension d and its norm as:

$$H^1(\Omega) = \{ f \in L^2(\Omega) \ \text{ st } \ \nabla f \in [L^2(\Omega)]^d \}, \qquad \|f\|^2_{H^1(\Omega)} = \|f\|^2_{L^2(\Omega)} + \|\nabla f\|^2_{L^2(\Omega)}.$$

In order to deal with Dirichlet boundary conditions we had to introduce the first order Sobolev space for vanishing boundary functions and its norm:

$$H^1_0(\Omega) = \{ f \in H^1(\Omega) \ \text{ st } \ f|_{\partial\Omega} = 0 \}, \qquad \|f\|_{H^1_0(\Omega)} = \|\nabla f\|_{L^2(\Omega)},$$

this space is complete with respect to the Dirichlet norm that we know to be equivalent to the $H^1(\Omega)$ norm for each $f \in H^1_0(\Omega)$. Since we were also interested in vector valued functions under the incompressible constrain, we introduced the canonical space used to deal with these kind of functions:

$$\boldsymbol{H}(\operatorname{div}; \Omega) = \{ \boldsymbol{\tau} \in [L^2(\Omega)]^d \ \text{ st } \ \operatorname{div} \boldsymbol{\tau} \in L^2(\Omega) \},$$

this space is endowed with the norm

$$\|\boldsymbol{f}\|^2_{\boldsymbol{H}(\operatorname{div};\Omega)} = \|\boldsymbol{f}\|^2_{L^2(\Omega)} + \|\operatorname{div} \boldsymbol{f}\|^2_{L^2(\Omega)}.$$

This norm was fundamental for the Darcy problem since we wanted to control both $\boldsymbol{u}$ and $\operatorname{div} \boldsymbol{u}$ for stability purposes. In order to be able to write finite dimensional formulations we introduced the *mesh* that discretized our domain Ω. We simply considered a partition in the form:

$$\overline{\Omega} = \bigcup_{\mathcal{K} \in \mathcal{T}} \overline{\mathcal{K}}$$

where each $\mathcal{K} \in \mathcal{T}$ is called *mesh element*. We recall to the readers that in order to deal with complex geometry a non conforming mesh is the most suitable choice since it discretize the domain with fewer constrains respect to conforming meshes. The only problem that arises is to find a method that can handle this type of mesh, hence the choice of exploiting dG methods (more on

[7]). Along with the definition of mesh we introduced the *diameter* of a generic element $h_{\mathcal{K}}$ and the *meshsize* h, namely:

$$h := \max_{\mathcal{K}\in\mathcal{T}} h_{\mathcal{K}} \, .$$

We denoted by $\mathcal{T}_h$ a mesh $\mathcal{T}$ with meshsize h. For each mesh element $\mathcal{K} \in \mathcal{T}_h$, we introduced the unit *outward normal* $\boldsymbol{n}_{\mathcal{K}}$ defined almost everywhere on $\partial\mathcal{K}$. As a matter of notations the unit outward normal can also be expressed as $\boldsymbol{n}^+$ or $\boldsymbol{n}^-$ accordingly to the two possible orientations, in Fig 2.1 we can observe an example. In order to take into consideration boundary values and interfaces values we collected in a couple of sets all the mesh faces, specifically the set $\mathcal{F}_h^I$ contains all the common interfaces between two elements, instead the set $\mathcal{F}_h^B$ contains all the boundary faces. Lastly we introduced a third set: $\mathcal{F}_h = \mathcal{F}_h^I \cup \mathcal{F}_h^B$ that collects all the faces of the mesh. We then defined the average and the jump operators on elements' edges, it is by means of these operators that the discontinuous formulation of the problem is possible. We considered a generic scalar-valued function v and a generic vector-valued function $\boldsymbol{\tau}$ both defined over Ω, then the *average* of a function is defined as:

$$\begin{aligned} \{\!\{v\}\!\} &= \frac{v^+ + v^-}{2} & \{\!\{\boldsymbol{\tau}\}\!\} &= \frac{\boldsymbol{\tau}^+ + \boldsymbol{\tau}^-}{2} & \forall F \in \mathcal{F}_h^I \, , \\ \{\!\{v\}\!\} &= v & \{\!\{\boldsymbol{\tau}\}\!\} &= \boldsymbol{\tau} & \forall F \in \mathcal{F}_h^B \, , \end{aligned}$$

and the *jump* as:

$$\begin{aligned} [\![v]\!] &= v^+\boldsymbol{n}^+ + v^-\boldsymbol{n}^- & [\![\boldsymbol{\tau}]\!] &= \boldsymbol{\tau}^+ \cdot \boldsymbol{n}^+ + \boldsymbol{\tau}^- \cdot \boldsymbol{n}^- & \forall F \in \mathcal{F}_h^I \, , \\ [\![v]\!] &= v\boldsymbol{n} & [\![\boldsymbol{\tau}]\!] &= \boldsymbol{\tau} \cdot \boldsymbol{n} & \forall F \in \mathcal{F}_h^B \, . \end{aligned}$$

By means of these operators and some algebraic manipulations it can be proven a well-known result which we will use to write the discrete formulation of the problems, this result goes under the name of *magic formula* (Ref. Arnold 1982):

$$\sum_{\mathcal{K}\in\mathcal{T}_h} \int_{\partial\mathcal{K}} \boldsymbol{\tau} \cdot \boldsymbol{n}_{\mathcal{K}} v = \sum_{F\in\mathcal{F}_h} \int_F \{\!\{\boldsymbol{\tau}\}\!\} \cdot [\![v]\!] + \sum_{F\in\mathcal{F}_h^I} \int_F [\![\boldsymbol{\tau}]\!] \{\!\{v\}\!\} \, , \tag{2.3}$$

being $\boldsymbol{\tau}$ and v sufficiently regular vector and scalar valued functions respectively. In order to discuss dG formulations we introduced some spaces containing discontinuous functions, these spaces will play a core role in the discrete formulation. Let $\mathcal{T}_h$ be a mesh of the domain, we presented the *broken Sobolev spaces* defined over the mesh:

$$H^1(\mathcal{T}_h) = \{f \in L^2(\Omega) \text{ st } \forall \mathcal{K} \in \mathcal{T}_h \, , \; f|_{\mathcal{K}} \in H^1(\mathcal{K})\} \, ,$$

endowed with the norms

$$\begin{aligned} \|v\|^2_{L^2(\mathcal{F}_h)} &= \sum_{\mathcal{F}\in\mathcal{F}_h} \|v\|^2_{L^2(F)} \, , \\ \|v\|^2_{H^1(\mathcal{T}_h)} &= \sum_{\mathcal{K}\in\mathcal{T}_h} \|v\|^2_{H^1(\mathcal{K})} \, , \end{aligned}$$

called *skeleton norm* and H^1 *broken norm* respectively, and

$$\boldsymbol{H}(\mathrm{div};\mathcal{T}_h) = \{\boldsymbol{\tau} \in [L^2(\Omega)]^d \text{ st } \forall \mathcal{K} \in \mathcal{T}_h, \; \boldsymbol{\tau}|_{\mathcal{K}} \in \boldsymbol{H}(\mathrm{div};\mathcal{K})\}$$

endowed with the L^2 broken norm. Likewise we presented the *space of broken polynomials of order* n for both scalar and vector functions:

$$\mathbb{P}^n(\mathcal{T}_h) = \{f \in L^2(\Omega) \;\text{ st }\; \forall \mathcal{K} \in \mathcal{T}_h, \; f|_{\mathcal{K}} \in \mathbb{P}^n(\mathcal{K})\} \, ,$$

$$[\mathbb{P}^n(\mathcal{T}_h)]^d = \{\boldsymbol{\tau} \in [L^2(\Omega)]^d \;\text{ st }\; \forall \mathcal{K} \in \mathcal{T}_h, \; \boldsymbol{\tau}|_{\mathcal{K}} \in [\mathbb{P}^n(\mathcal{K})]^d\} \, .$$

All the notations adopted come from [3],[5] and [6].

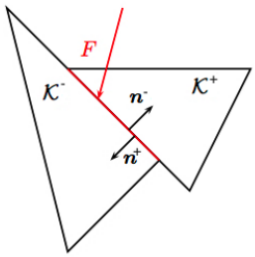

Figure 2.1: Example of two adjacent elements. Figure taken from the book: *"Numerical Models for Differential Problems"* by Alfio Quarteroni [5]

2.2 dG formulation transport-diffusion problem

The purpose of this section was to derive the discrete formulation of (2.2), but, instead of the non-conservative form we started by the conservative one

$$-\kappa\Delta\theta + \mathrm{div}(\boldsymbol{u}\theta) = g$$

We made this choice because the conservative formulation let us to integrate by parts, however it can be observe that the two formulations are equivalent under the condition $\mathrm{div}\boldsymbol{u} = 0$, since the underlying equality holds true:

$$\mathrm{div}(\theta\,\boldsymbol{u}) = \theta\,\mathrm{div}(\boldsymbol{u}) + \boldsymbol{u}\cdot\nabla\theta\,.$$

One may think that asking $\mathrm{div}\boldsymbol{u} = 0$ is a very restrictive assumption, but we recall that in the strong form of the final problem the divergence-free constrain is a given equation. Despite that, when we deal with the numerical approximation $\boldsymbol{u}_h$, we can not assume its divergence to be exactly zero. We overcame this issue by choosing the finite dimensional space for velocity in such a way that $\mathrm{div}\boldsymbol{u}_h \approx 0$, namely by taking the finite dimensional space as a subspace of $\boldsymbol{H}(\mathrm{div};\Omega)$, but we will discuss this issue in more details later in the report. Under this assumption we could work as if the incompressibility condition were satisfied also for the discrete problem. Nevertheless, a portion of the final error will be due to this approximation.

Let $\mathcal{T}_h$ be a generic mesh defined over the domain Ω. Let $\theta \in H^1_0(\Omega)\cap H^2(\Omega)$ and $\boldsymbol{u}\in\boldsymbol{H}(\mathrm{div};\Omega)$, moreover let $V = H^1(\mathcal{T}_h)$ the broken Sobolev space of order one defined over the mesh. By following the canonical procedure we took an a arbitrary test function $v\in V$, we multiplied the equation times v and we integrated over Ω, then we rephrased the integrals as sums of integrals over the elements $\mathcal{K}\in\mathcal{T}_h$ and subsequently we integrated by parts the "local integrals", obtaining:

$$\sum_{\mathcal{K}\in\mathcal{T}_h}\int_{\mathcal{K}}\kappa\nabla_h\theta\cdot\nabla_h v - \sum_{\mathcal{K}\in\mathcal{T}_h}\int_{\partial\mathcal{K}}\kappa v\,\nabla_h\theta\cdot\boldsymbol{n}_{\mathcal{K}} - \sum_{\mathcal{K}\in\mathcal{T}_h}\int_{\mathcal{K}}\boldsymbol{u}\theta\cdot\nabla_h v + \sum_{\mathcal{K}\in\mathcal{T}_h}\int_{\partial\mathcal{K}}(\theta\boldsymbol{u})\cdot\boldsymbol{n}_{\mathcal{K}}\,v = \int_\Omega gv$$

We carried on the deduction by applying (2.3) to the two terms that take into account the interfaces values:

$$\sum_{\mathcal{K}\in\mathcal{T}_h}\int_{\mathcal{K}}\kappa\nabla_h\theta\cdot\nabla_h v - \sum_{F\in\mathcal{F}_h}\int_F\{\!\{\kappa\nabla_h\theta\}\!\}\cdot[\![v]\!] - \sum_{\mathcal{K}\in\mathcal{T}_h}\int_{\mathcal{K}}\boldsymbol{u}\theta\cdot\nabla_h v + \sum_{F\in\mathcal{F}_h}\int_F\{\!\{\theta\boldsymbol{u}\}\!\}\cdot[\![v]\!] = \int_\Omega gv\,.$$

In the previous equations, by the symbol $\nabla_h(\cdot)$ we mean the element wise gradient operator:

$$(\nabla_h v)|_{\mathcal{K}} = \nabla(v|_{\mathcal{K}})\ \forall\mathcal{K}\in\mathcal{T}_h\,.$$

Let the readers observe that the terms

$$-\sum_{F\in\mathcal{F}_h^I}\int_F[\![\kappa\nabla_h\theta]\!]\,\{\!\{v\}\!\} \qquad \text{and} \qquad +\sum_{F\in\mathcal{F}_h^I}\int_F[\![\boldsymbol{u}\theta]\!]\,\{\!\{v\}\!\}$$

coming from the magic formula are null thanks to the assumptions on θ and $\boldsymbol{u}$, for the second in particular we refer to Lemma 1.24 in [3]. In order to reach a well-posed formulation we had to add two strongly consistent terms for the diffusive part of the equation, one for symmetrization and one for stabilization of jumps, these quantities provide greater generality and improve the stability of the method:

$$-\sum_{F\in\mathcal{F}_h}\int_F \{\!\{\kappa\nabla_h v\}\!\}\cdot[\![\theta]\!] \quad \text{symmetrization term;} \qquad +\sum_{F\in\mathcal{F}_h}\int_F \gamma\,[\![\theta]\!]\cdot[\![v]\!] \quad \text{stabilization term.}$$

We chosen to treat the symmetrization term with the *symmetric interior penalty* (SIP method) and the stabilization term with the following value for γ:

$$\gamma=\alpha\frac{r^2}{h}\,,\qquad r=\begin{cases}\max\{r_{\mathcal{K}}^-,r_{\mathcal{K}}^+\}, & \text{if } F\in\mathcal{F}_h^I\\ r_{\mathcal{K}}, & \text{if } F\in\mathcal{F}_h^B\end{cases}\qquad h=\begin{cases}\min\{h_{\mathcal{K}}^-,h_{\mathcal{K}}^+\}, & \text{if } F\in\mathcal{F}_h^I\\ h_{\mathcal{K}}, & \text{if } F\in\mathcal{F}_h^B\end{cases}$$

where α is a parameter to be chosen. If we only had the diffusion part, to have stability and well-posedness of the problem, it would have been enough to choose the parameter α " sufficiently large". From theory we know that the values of α that bring stability for the SIP method hovers around 10, nevertheless its optimal value is not known, so in practice a parameter tuning is required. In order to achieve stability the usual procedure is to replace the average in the transport term with an upwinding average. Since in the formulation we also had a diffusion part, where a stabilization of jumps was already performed (stabilization term), we decided to introduce a more versatile stabilization proposed by Brezzi, Marini and Suli in [2]. This term basically adds a penalty term on the internal faces with a parameter that can be tuned.

$$+\sum_{F\in\mathcal{F}_h^I}\int_F c\,[\![\theta]\!]\,[\![v]\!]\,,\qquad c=\frac{|\boldsymbol{u}\cdot\boldsymbol{n}_{\mathcal{K}}|}{2}$$

At the denominator in the definition of c it can been put any positive coefficient, but if it is chosen 2 this term will be exactly equivalent to the usual upwinding average [2]. Then we imposed the Dirichlet boundary condition $\theta=\theta_0$ on the jumps of the diffusion terms and on the averages of the transport terms.

We obtained a well-posed formulation (see [3], Section 4.6.2), however our final goal was to exploit this equation in a bigger system, so we needed something more. A key property that we wanted our discrete bilinear form to satisfy was skew-symmetry.

Definition. *Given $L: V\times V\to\mathbb{R}$, it is said to be skew-symmetric if $L(u,u)=0\ \ \forall u\in V$*

This property is an additional request which is not mandatory for the well-posedness of the diffusion-transport problem, in fact well-posedness can be achieved simply by proving coercivity with respect to the energy norm. However this property is really useful to find some a priori bounds for the complete problem. Moreover, in order to prove coercivity, we need some assumptions on $\boldsymbol{u}$ that are not guaranteed if $\boldsymbol{u}$ is the solution of Darcy-Forchheimer. To obtain a skew-symmetric form we added to the left hand side the following terms

$$-\frac{1}{2}\sum_{\mathcal{K}\in\mathcal{T}_h}\int_{\mathcal{K}}\mathrm{div}\boldsymbol{u}\;\theta v\;+\;\frac{1}{2}\sum_{F\in\mathcal{F}_h^B}\int_F\boldsymbol{u}\cdot\boldsymbol{n}\;\theta v \tag{2.4}$$

and to the right hand side

$$+\frac{1}{2}\sum_{F\in\mathcal{F}_h^B}\int_F\boldsymbol{u}\cdot\boldsymbol{n}\;\theta_0 v\,. \tag{2.5}$$

The first term in (2.4) is consistent since we assumed the incompressibility condition and the second one in (2.4) is consistent coupled with the new term on the right hand side. So, by gathering all the terms we have

$$\begin{aligned}&a_h(\cdot\,,\cdot)\;:\;V\times V\to\mathbb{R}\,,\\ &b_h(\cdot\,,\cdot)\;:\;V\times V\to\mathbb{R}\,,\\ &l_h(\cdot)\;:\;V\to\mathbb{R}\,.\end{aligned}$$

Where the bilinear form $a_h(\cdot,\cdot)$ takes into account the terms from the diffusive component of the equation, instead the bilinear form $b_h(\cdot,\cdot)$ the ones from the transport component. $l_h(\cdot)$ is the functional. They are defined as:

$$\begin{aligned} a_h(\theta,v) = &\sum_{\mathcal{K}\in\mathcal{T}_h}\int_{\mathcal{K}}\kappa\nabla_h\theta\cdot\nabla_h v - \sum_{F\in\mathcal{F}_h}\int_F \{\!\{\kappa\nabla_h\theta\}\!\}\cdot[\![v]\!] - \sum_{F\in\mathcal{F}_h^I}\int_F \{\!\{\kappa\nabla_h v\}\!\}\cdot[\![\theta]\!] \\ &- \sum_{F\in\mathcal{F}_h^B}\int_F \kappa\nabla_h v\cdot\boldsymbol{n}\theta + \sum_{F\in\mathcal{F}_h^I}\int_F (\gamma+c)\,[\![\theta]\!]\cdot[\![v]\!] + \sum_{F\in\mathcal{F}_h^B}\int_F \gamma\,\theta\,v \end{aligned} \tag{2.6}$$

$$\begin{aligned} b_h(\theta,v) = &-\sum_{\mathcal{K}\in\mathcal{T}_h}\int_{\mathcal{K}}\boldsymbol{u}\theta\cdot\nabla_h v + \sum_{F\in\mathcal{F}_h^I}\int_F \{\!\{\theta\boldsymbol{u}\}\!\}\cdot[\![v]\!] + \frac{1}{2}\sum_{F\in\mathcal{F}_h^B}\int_F \boldsymbol{u}\cdot\boldsymbol{n}\theta v \\ &- \frac{1}{2}\sum_{\mathcal{K}\in\mathcal{T}_h}\int_{\mathcal{K}}\mathrm{div}\boldsymbol{u}\;\theta v \end{aligned} \tag{2.7}$$

$$\begin{aligned} l_h(v) = &\int_\Omega gv \;\; - \sum_{F\in\mathcal{F}_h^B}\int_F \kappa\nabla_h v\cdot\boldsymbol{n}\theta_0 \;\; + \sum_{F\in\mathcal{F}_h^B}\int_F \theta_0 v\gamma \;- \sum_{F\in\mathcal{F}_h^B}\int_F \boldsymbol{u}\cdot\boldsymbol{n}\,\theta_0 v \\ &+ \frac{1}{2}\sum_{F\in\mathcal{F}_h^B}\int_F \boldsymbol{u}\cdot\boldsymbol{n}\,\theta_0 v \end{aligned} \tag{2.8}$$

Remark. The last two terms on the right hand side can be summed (as it is done in the code). We left them separated in order to isolate the terms that we added. Moreover we summed in a_h the stabilization term from Brezzi, Marini, Suli with the stabilization term for diffusion.

Proposition 1. *$b_h(\cdot,\cdot) : V\times V\to\mathbb{R}$ is skew-symmetric*

Proof. Let us consider this quantity

$$-\sum_{\mathcal{K}\in\mathcal{T}_h}\int_{\mathcal{K}}\boldsymbol{u}\theta\cdot\nabla_h v + \sum_{F\in\mathcal{F}_h^I}\int_F \{\!\{\theta\boldsymbol{u}\}\!\}\cdot[\![v]\!] \tag{2.9}$$

Which is $b_h(\theta,v)$ without the two additive terms of (2.4). Then we split the first term into two equal parts:

$$-\frac{1}{2}\sum_{\mathcal{K}\in\mathcal{T}_h}\int_{\mathcal{K}}\boldsymbol{u}\theta\cdot\nabla_h v - \frac{1}{2}\sum_{\mathcal{K}\in\mathcal{T}_h}\int_{\mathcal{K}}\boldsymbol{u}\theta\cdot\nabla_h v + \sum_{F\in\mathcal{F}_h^I}\int_F \{\!\{\theta\boldsymbol{u}\}\!\}\cdot[\![v]\!] \tag{2.10}$$

we exploit the equality $\mathrm{div}(\boldsymbol{u}v) = \boldsymbol{u}\cdot\nabla v + \mathrm{div}\boldsymbol{u}\;v$ and we get

$$-\frac{1}{2}\sum_{\mathcal{K}\in\mathcal{T}_h}\int_{\mathcal{K}}\boldsymbol{u}\theta\cdot\nabla_h v - \frac{1}{2}\sum_{\mathcal{K}\in\mathcal{T}_h}\int_{\mathcal{K}}\mathrm{div}(\boldsymbol{u}v)\;\theta + \frac{1}{2}\sum_{\mathcal{K}\in\mathcal{T}_h}\int_{\mathcal{K}}\mathrm{div}\boldsymbol{u}\;v\theta + \sum_{F\in\mathcal{F}_h^I}\int_F \{\!\{\theta\boldsymbol{u}\}\!\}\cdot[\![v]\!] \tag{2.11}$$

Now we can integrate by parts the second term. We exploit the magic formula for the integrals over the boundaries of the elements, moreover we split in two the last term. We get:

$$\begin{aligned} &-\frac{1}{2}\sum_{\mathcal{K}\in\mathcal{T}_h}\int_{\mathcal{K}}\boldsymbol{u}\theta\cdot\nabla_h v - \frac{1}{2}\sum_{F\in\mathcal{F}_h}\int_F \{\!\{\theta\boldsymbol{u}\}\!\}\cdot[\![v]\!] - \frac{1}{2}\sum_{F\in\mathcal{F}_h^I}\int_F [\![\theta\boldsymbol{u}]\!]\cdot\{\!\{v\}\!\} + \frac{1}{2}\sum_{\mathcal{K}\in\mathcal{T}_h}\int_{\mathcal{K}}\boldsymbol{u}v\cdot\nabla_h\theta \\ &+\frac{1}{2}\sum_{\mathcal{K}\in\mathcal{T}_h}\int_{\mathcal{K}}\mathrm{div}\boldsymbol{u}\;v\theta + \frac{1}{2}\sum_{F\in\mathcal{F}_h^I}\int_F \{\!\{\theta\boldsymbol{u}\}\!\}\cdot[\![v]\!] + \frac{1}{2}\sum_{F\in\mathcal{F}_h^I}\int_F \{\!\{\theta\boldsymbol{u}\}\!\}\cdot[\![v]\!] \end{aligned} \tag{2.12}$$

We notice that from the difference between the 2^{nd} and the 6^{th} term we are left with the sum of the integrals over the boundary faces. If we now take $v=\theta$ also the 1^{st} term and the 4^{th} terms cancel out. We are left with

$$-\frac{1}{2}\sum_{F\in\mathcal{F}_h^B}\int_F \{\!\{\theta\boldsymbol{u}\}\!\}\cdot[\![\theta]\!] - \frac{1}{2}\sum_{F\in\mathcal{F}_h^I}\int_F [\![\theta\boldsymbol{u}]\!]\cdot\{\!\{\theta\}\!\} + \frac{1}{2}\sum_{\mathcal{K}\in\mathcal{T}_h}\int_{\mathcal{K}}\mathrm{div}\boldsymbol{u}\;\theta^2 + \frac{1}{2}\sum_{F\in\mathcal{F}_h^I}\int_F \{\!\{\theta\boldsymbol{u}\}\!\}\cdot[\![\theta]\!]\;. \tag{2.13}$$

If we add the first term of (2.4) the third term cancels. For the second and the fourth terms it can be also proved that for any $\boldsymbol{u} \in \boldsymbol{H}(\mathrm{div}; \Omega)$:

$$\sum_{F \in \mathcal{F}_h^I} \int_F [\![\theta \boldsymbol{u}]\!] \cdot \{\!\{\theta\}\!\} = \sum_{F \in \mathcal{F}_h^I} \int_F \{\!\{\theta \boldsymbol{u}\}\!\} \cdot [\![\theta]\!] \tag{2.14}$$

This leads to only one term remaining, that is

$$-\frac{1}{2} \sum_{F \in \mathcal{F}_h^B} \int_F \{\!\{\theta \boldsymbol{u}\}\!\} \cdot [\![\theta]\!] \tag{2.15}$$

which is exactly the opposite of the second term in (2.4). Finally if we add to (2.9) the two terms of (2.4) and we repeat the same argument we will get exactly zero, hence skew-symmetry is proved. □

Definition. $\|v\|_{DG}^2 := \|\nabla_h v\|_{L^2(\Omega)}^2 + \|\sqrt{\gamma}\,[\![v]\!]\,\|_{L^2(\mathcal{F}_h)}^2$

Proposition 2. *$c_h(\cdot\,,\cdot) := a_h(\cdot\,,\cdot) + b_h(\cdot\,,\cdot)$ is coercive with respect to the DG-norm*

Proof. Let's test c_h by taking $v = \theta$, we get

$$c_h(\theta, \theta) = a_h(\theta, \theta) + b_h(\theta, \theta) \tag{2.16}$$

by Prop.1 we know that $b_h(\theta, \theta) = 0$ and from [3], Lemma 4.51, we know that a_h is coercive with respect to the DG-norm. Here we have that $\tilde{\gamma} := \gamma + c$ and the final result is

$$C\|\theta\|_{DG}^2 \leq a_h(\theta, \theta) = c_h(\theta, \theta) \tag{2.17}$$

Where the γ appearing in the definition of the DG-norm is actually $\tilde{\gamma}$ □

Thanks to these results we were able to prove the well-posedness of this new formulation of the problem, always keeping in mind that it only works if the incompressibility condition is fulfilled (at least numerically). Finally we defined $V_h = \mathbb{P}^r(\mathcal{T}_h)$ and we wrote the discrete formulation of the problem, which reads:

$$\text{Find } \theta_h \in V_h \text{ s.t. } a_h(\theta_h, v_h) + b_h(\theta_h, v_h) = l_h(v_h) \quad \forall v_h \in V_h\,. \tag{2.18}$$

Proof. (of 2.14)

$$\begin{aligned}
&\sum_{F \in \mathcal{F}_h^I} \int_F \{\!\{\theta \boldsymbol{u}\}\!\} \cdot [\![\theta]\!] - \sum_{F \in \mathcal{F}_h^I} \int_F [\![\theta \boldsymbol{u}]\!] \cdot \{\!\{\theta\}\!\} = \\
&\frac{(\theta \boldsymbol{u})^+ + (\theta \boldsymbol{u})^-}{2} \cdot (\theta^+ \boldsymbol{n}^+ + \theta^- \boldsymbol{n}^-) - ((\theta \boldsymbol{u})^+ \cdot \boldsymbol{n}^+ + (\theta \boldsymbol{u})^- \cdot \boldsymbol{n}^-) \frac{\theta^+ + \theta^-}{2} = \\
&\frac{1}{2} \left(\theta^{+^2} \boldsymbol{u}^+ \cdot \boldsymbol{n}^+ + \theta^+ \theta^- \boldsymbol{u}^+ \cdot \boldsymbol{n}^- + \theta^- \theta^+ \boldsymbol{u}^- \cdot \boldsymbol{n}^+ + \theta^{-^2} \boldsymbol{u}^- \cdot \boldsymbol{n}^- \right) \\
&- \frac{1}{2} \left(\theta^{+^2} \boldsymbol{u}^+ \cdot \boldsymbol{n}^+ + \theta^- \theta^+ \boldsymbol{u}^- \cdot \boldsymbol{n}^+ + \theta^+ \theta^- \boldsymbol{u}^+ \cdot \boldsymbol{n}^- + \theta^{-^2} \boldsymbol{u}^- \cdot \boldsymbol{n}^- \right) = 0
\end{aligned}$$

□

2.3 Numerical experiments transport-diffusion problem

In this section we presented the implementation of problem (2.18) and its numerical behaviors. The code language we used is Python and the library that we exploited is the FEniCS library, an open-source computing platform for solving partial differential equations. This will be the main environment for all the parts of the project concerning numerical simulations. Every theoretical part is followed by numerical experiments, whose aim is to assess the performances of the methods. Our goals were to understand if our algorithms were able to give reliable solutions and also to set some benchmark results for more advanced analysis and implementations.

Definition. *A mesh $\mathcal{T}_h$ is said to be conforming if the intersection between two arbitrary elements $\mathcal{K}$ is a subelement (edge, vertex) or nothing.*

Definition. *A mesh $\mathcal{T}_h$ is said to be uniform if all the elements $\mathcal{K} \in \mathcal{T}_h$ have approximately the same diameter $h_{\mathcal{K}}$.*

We set the domain as the unit two dimensional square $\Omega = (0,1) \times (0,1)$ and we considered a uniform conforming mesh $\mathcal{T}_h$. The finite element space chosen for the (2.18) is the space of broken polynomials $V_h = \mathbb{P}^r(\mathcal{T}_h)$, where we set $r = 1$. The first test we implemented is characterized by the following data:

$$\boldsymbol{u} = [1,1]^T\,, \quad g \equiv 0\,, \quad \theta_{ex} = \frac{e^{\frac{x-1}{\kappa}} - e^{-\frac{1}{\kappa}}}{1 - e^{-\frac{1}{\kappa}}} + \frac{e^{\frac{y-1}{\kappa}} - e^{-\frac{1}{\kappa}}}{1 - e^{-\frac{1}{\kappa}}}\,, \quad \alpha = 9.1\,,$$

with boundary conditions that are inferred from the exact solution and two different values for the parameter κ that we considered constant all over the domain. It is important to point out that all the test we performed are with values of $\boldsymbol{u}$ s.t. $\mathrm{div}\boldsymbol{u} = 0$. For the details on the implementation we refer to the Python script named: "STEP1-DiffusionTransport", where the code is commented. We report now our results.

Remark: In this report all the plots that display orders of convergence are rescaled by the first error of the series, namely the error computed for the first refinement (If different it will be specified). This choice was done in order to visualize better the trends. Unfortunately in this way it's not possible to have an idea of the absolute values of the errors, hence we decided to gather them in tables.

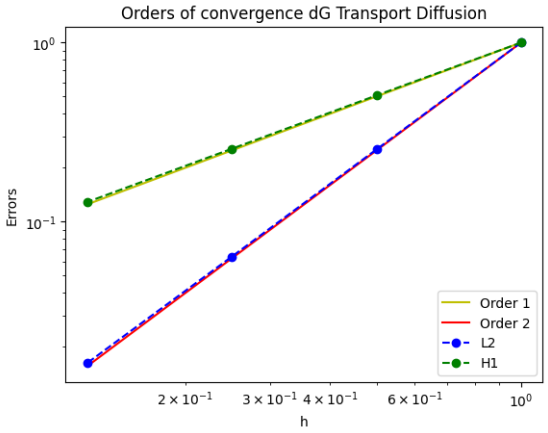

Figure 2.2: $\kappa = 0.05\,,\ \mathbb{P}e = 1.414$

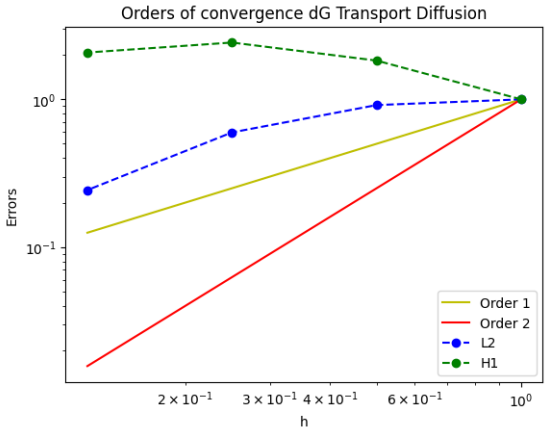

Figure 2.3: $\kappa = 1 \times 10^{-6}\,,\ \mathbb{P}e = 7.071 \times 10^6$

h	$\|\|\theta - \theta_h\|\|_{L^2}$	$\|\|\theta - \theta_h\|\|_{H^1}$
$\frac{1}{32}$	3.723×10^{-3}	6.225×10^{-1}
$\frac{1}{64}$	9.428×10^{-4}	3.156×10^{-1}
$\frac{1}{128}$	2.379×10^{-4}	1.590×10^{-1}
$\frac{1}{256}$	6.151×10^{-5}	8.082×10^{-2}

Table 2.1: $\kappa = 0.05\,,\ \mathbb{P}e = 1.414$

h	$\|\|\theta - \theta_h\|\|_{L^2}$	$\|\|\theta - \theta_h\|\|_{H^1}$
$\frac{1}{32}$	5.832	9.535×10^2
$\frac{1}{64}$	5.335	1.746×10^3
$\frac{1}{128}$	3.482	2.312×10^3
$\frac{1}{256}$	1.417	1.979×10^3

Table 2.2: $\kappa = 1 \times 10^{-6}\,,\ \mathbb{P}e = 7.071 \times 10^6$

On the left (Fig. 2.2, Tab. 2.1) we reported the orders of convergence and the errors of the numerical experiment with thermal conductivity κ equal to 0.05, instead on the right (Fig. 2.3, Tab. 2.2) the results correspondent to a thermal conductivity equal to 1×10^{-6}. As it can be seen we reached an order of convergence equals to 2 for the L^2 norm and an order equal to 1 for the H^1 norm for $\kappa = 0.05$, these results are in agreement with the theory. We also recall to the readers that the H^1 norm and DG norm behave in the same way, hence they have the same order of accuracy. We obtained poor results instead for the advection dominant case $\kappa = 1 \times 10^{-6}$, this is probably due to the fact that our implementation can not handle problems related to a very high Peclet number. However, from the physical point of view, the thermal conductivity can not be below the threshold of 1×10^{-4} (value that will be tested in the second experiment), hence we took note of this behaviour but moved on with our experiments since we were only interested in physically meaningful coefficients.

Subsequently we decided to slightly increase the complexity of the experiment by introducing a non-trivial force and a non-constant transport coefficient; moreover we increased the Peclet number by picking a smaller (yet physically interesting) thermal conductivity κ; the values of the parameters have been changed in the following:

$$\kappa = 1 \times 10^{-4}\,, \quad \boldsymbol{u} = [y, x]^T\,, \quad g = -4\kappa + 4xy\,, \quad \theta_{ex} = x^2 + y^2\,, \quad \alpha = 9.1\,.$$

Again we emphasize that $\mathrm{div}\boldsymbol{u} = 0$. Exploiting the already implemented function we obtained the results reported in Figure 2.4 and Table 2.3. By looking to these results we can conclude that our discontinuous implementation can stand to low values of thermal conductivity without losing any accuracy. We still see an order of convergence equal to 2 for the L^2 norm and an order equal to 1 for the H^1 norm. We then decided to increase the degree of the discrete space to two ($r = 2$), hence we set $V_h = \mathbb{P}^2(\mathcal{T}_h)$. As it can be seen in Figure 2.5 we did not get an increase on the order of convergence in neither one of the two norms, we assumed that this behaviour was related to the presence of the additional terms that bring skew-symmetry in the bilinear form $b(\cdot, \cdot)$. However, we achieve very low errors as can be seen in Table 2.4, this is probably because we were approximating the exact solution θ_{ex} with a polynomial of the same order.

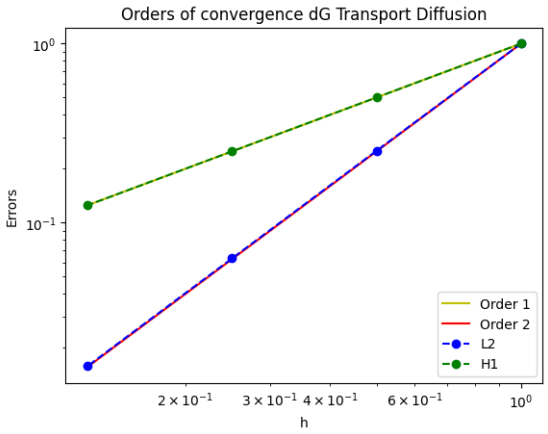

Figure 2.4: $\kappa = 1 \times 10^{-4}\,,\ r = 1$

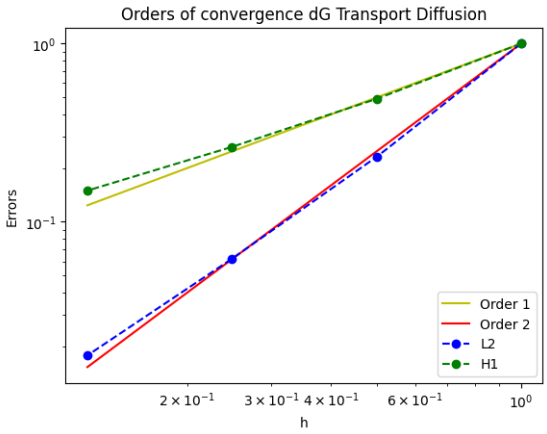

Figure 2.5: $\kappa = 1 \times 10^{-4}\,,\ r = 2$

h	$\|\|\theta-\theta_h\|\|_{L^2}$	$\|\|\theta-\theta_h\|\|_{H^1}$
$\frac{1}{20}$	1.808×10^{-4}	2.359×10^{-2}
$\frac{1}{40}$	4.627×10^{-5}	1.179×10^{-2}
$\frac{1}{80}$	1.163×10^{-5}	5.893×10^{-3}
$\frac{1}{160}$	2.910×10^{-6}	2.946×10^{-3}

Table 2.3: $\kappa = 1\times10^{-4}$, $r=1$

h	$\|\|\theta-\theta_h\|\|_{L^2}$	$\|\|\theta-\theta_h\|\|_{H^1}$
$\frac{1}{20}$	9.972×10^{-8}	2.387×10^{-5}
$\frac{1}{40}$	2.040×10^{-8}	1.092×10^{-5}
$\frac{1}{80}$	5.327×10^{-9}	5.741×10^{-6}
$\frac{1}{160}$	1.493×10^{-9}	3.197×10^{-6}

Table 2.4: $\kappa = 1\times10^{-4}$, $r=2$

2.4 Discrete formulation Darcy problem

In our paper we discussed the Darcy problem in two versions according to the boundary condition we considered. If we impose a Dirichlet boundary condition $p = p_D$, after the definitions of the spaces $\boldsymbol{W} := \boldsymbol{H}(\mathrm{div};\Omega)$ and $Q := L^2(\Omega)$, we get the weak formulation:

$$\text{Find } (\boldsymbol{u},p)\in \boldsymbol{W}\times Q \text{ s.t. } \begin{cases} \int_\Omega \nu\boldsymbol{u}\cdot\boldsymbol{v} - \int_\Omega p\,\mathrm{div}\boldsymbol{v} = \int_\Omega \boldsymbol{f}\cdot\boldsymbol{v} - \int_{\partial\Omega} p_D\,\boldsymbol{n}\cdot\boldsymbol{v} & \forall \boldsymbol{v}\in\boldsymbol{W} \\ \int_\Omega q\,\mathrm{div}\boldsymbol{u} = 0 & \forall q\in Q \end{cases} \tag{2.19}$$

On the other hand, if we consider a Neumann Boundary condition $\boldsymbol{u}\cdot\boldsymbol{n}=0$ we need to define $\boldsymbol{W} := \{\boldsymbol{v}\in\boldsymbol{H}(\mathrm{div};\Omega) : \boldsymbol{v}\cdot\boldsymbol{n}|_{\partial\Omega}=0\}$, $Q := \{f\in L^2(\Omega) \,:\, \int_\Omega f = 0\} =: L^2_0(\Omega)$. The correspondent weak formulation reads:

$$\text{Find } (\boldsymbol{u},p)\in \boldsymbol{W}\times Q \text{ s.t. } \begin{cases} \int_\Omega \nu\boldsymbol{u}\cdot\boldsymbol{v} - \int_\Omega p\,\mathrm{div}\boldsymbol{v} = \int_\Omega \boldsymbol{f}\cdot\boldsymbol{v} & \forall \boldsymbol{v}\in\boldsymbol{W} \\ \int_\Omega q\,\mathrm{div}\boldsymbol{u} = 0 & \forall q\in Q \end{cases} \tag{2.20}$$

Both formulations are well-posed since both choices of spaces satisfy the inf-sup condition [8]. In the code we implemented only the first version so we will focus on that formulation in the following parts of the report. We introduced then the bilinear forms and the functional:

$$\begin{aligned} a(\cdot,\cdot) &: \boldsymbol{W}\times\boldsymbol{W}\to\mathbb{R} \qquad a(\boldsymbol{u},\boldsymbol{v}) = \int_\Omega \nu\boldsymbol{u}\cdot\boldsymbol{v} \\ b(\cdot,\cdot) &: \boldsymbol{W}\times Q\to\mathbb{R} \qquad b(\boldsymbol{v},q) = -\int_\Omega q\,\mathrm{div}\boldsymbol{v} \\ F(\cdot) &: \boldsymbol{W}\to\mathbb{R} \qquad F(\boldsymbol{v}) = \int_\Omega \boldsymbol{f}\cdot\boldsymbol{v} - \int_{\partial\Omega} p_D\,\boldsymbol{v}\cdot\boldsymbol{n} \end{aligned}$$

Thanks to these definitions we were able to write the weak formulation:

$$\text{Find } (\boldsymbol{u},p)\in \boldsymbol{W}\times Q \text{ st } \begin{cases} a(\boldsymbol{u},\boldsymbol{v}) + b(\boldsymbol{v},p) = F(\boldsymbol{v}) & \forall \boldsymbol{v}\in\boldsymbol{W} \\ b(\boldsymbol{u},q) = 0 & \forall q\in Q \end{cases} \tag{2.21}$$

The next step was to find a discrete approximation of (2.21). We introduced a conforming finite element partition $\mathcal{T}_h$ of the domain Ω. Then we set the finite dimensional spaces of trial and test functions for both the velocity field and pressure:

$$\mathbb{RT}^r(\mathcal{K}) = \mathbb{P}^r(\mathcal{K})^2 \bigoplus x\mathbb{P}^r(\mathcal{K})$$

$$\boldsymbol{W}_h = \{\boldsymbol{v}_h\in\boldsymbol{H}(\mathrm{div};\mathcal{T}_h),\ \ \boldsymbol{v}_h|_{\mathcal{K}}\in\mathbb{RT}^r(\mathcal{K}),\ \ \forall\mathcal{K}\in\mathcal{T}_h\}.$$

$$Q_h = \mathbb{P}^{r-1}(\mathcal{T}_h),$$

In particular, for the velocity space we used the well-know Raviart-Thomas elements of order r, these elements are conforming with respect to $\boldsymbol{W}$ and they lead to a discontinuous approximation of the velocity field (although the normal component is still continuous across the elements). For

pressure we used instead a set of piecewise polynomials of order $r-1$. In a natural way then we defined the discrete bilinear forms

$$a_h(\cdot,\cdot) : \boldsymbol{W}_h \times \boldsymbol{W}_h \to \mathbb{R}$$
$$b_h(\cdot,\cdot) : \boldsymbol{W}_h \times Q_h \to \mathbb{R}$$
$$F_h(\cdot) : \boldsymbol{W}_h \to \mathbb{R}$$

which are the discrete versions of the continuous counterparts. The discrete formulation of the problem reads:

$$\text{Find} \quad (\boldsymbol{u}_h, p_h) \in \boldsymbol{W_h} \times Q_h \quad st \quad \begin{cases} a_h(\boldsymbol{u}_h, \boldsymbol{v}_h) + b_h(\boldsymbol{v}_h, p_h) = F_h(\boldsymbol{v}_h) & \forall \boldsymbol{v}_h \in \boldsymbol{W}_h \\ b_h(\boldsymbol{u}_h, q_h) = 0 & \forall q_h \in Q_h \end{cases} \tag{2.22}$$

This problem is well-posed and the analysis uses the same techniques of the continuous version since the finite dimensional spaces are subspaces of the ∞-dimensional ones.

Remark: If we want to consider the Neumann boundary condition we can consider the same finite dimensional spaces, since the space of Raviart-Thomas elements is also a subspace of $\boldsymbol{W} = \{\boldsymbol{v} \in \boldsymbol{H}(\text{div}; \Omega) : \boldsymbol{v} \cdot \boldsymbol{n}|_{\partial\Omega} = 0\}$

2.5 Numerical experiments Darcy problem

The idea behind this experiment is pretty similar to the one made in section (**2.3**); we tested our implementation of problem (2.22) by performing a convergence test. We analyzed a simple situation in which the kinematic viscosity ν was taken as constant and the external body force $\boldsymbol{f}$ identically zero. After the definition of the conforming mesh $\mathcal{T}_h$ we defined the following data:

$$\Omega = (0,1) \times (0,1)\,, \quad \nu = 10\,, \quad \boldsymbol{f} = [0,0]^T\,, \quad p_{ex} = xy\,, \quad \boldsymbol{u}_{ex} = \left[-\frac{1}{\nu}y, -\frac{1}{\nu}x\right]^T\,, \quad r = 1$$

where r denotes the order of the discrete spaces presented in the previous paragraph, thus for the implementation we used elements of Raviart-Thomas of order one and piecewise constants to approximate the pressure. The results of this experiment are reported in the Figure 2.6 and Table 2.5. For both the unknowns we obtained an order of converge equal to 1 with respect to the L^2 norm, this result is in agreement with the theory since we set $r = 1$. After the first attempt we decided then to increase the order of the discrete spaces to $r = 2$. We achieved an order of convergence equal to 2 for the L^2 norm of the pressure, moreover the error of the velocity $\boldsymbol{u}_h$ reached the machine precision, therefore it no longer made sense to discuss its order of convergence, thus we did not represent it in the plot (Fig. 2.7, Tab 2.6). It is worthy to note that the aforementioned error increases with the refinement of the mesh, this is a correct behaviour since with a more finite mesh we introduce more computation hence, in this case, more errors associated to the roundoff. We reached the machine epsilon since we took $\boldsymbol{u}_{ex} \in \boldsymbol{W}_h$.

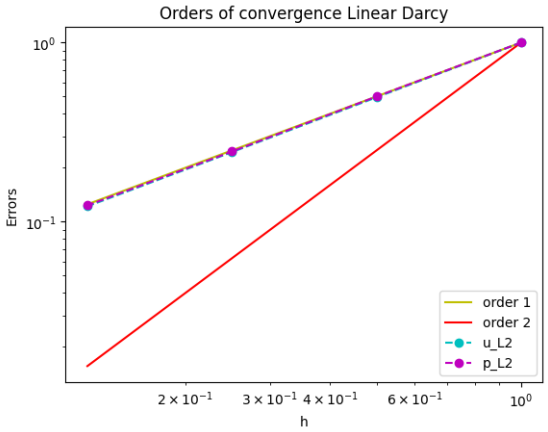

Figure 2.6: $r = 1$

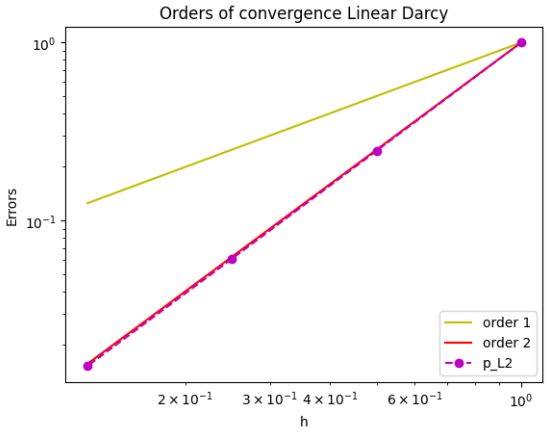

Figure 2.7: $r = 2$

h	$\|\|\boldsymbol{u}_{ex} - \boldsymbol{u}_h\|\|_{L^2}$	$\|\|p_{ex} - p_h\|\|_{L^2}$
$\frac{1}{20}$	2.005×10^{-3}	7.900×10^{-3}
$\frac{1}{40}$	9.919×10^{-4}	3.946×10^{-3}
$\frac{1}{80}$	4.905×10^{-4}	1.947×10^{-3}
$\frac{1}{160}$	2.442×10^{-5}	9.732×10^{-4}

Table 2.5: $r = 1$

h	$\|\|\boldsymbol{u}_{ex} - \boldsymbol{u}_h\|\|_{L^2}$	$\|\|p_{ex} - p_h\|\|_{L^2}$
$\frac{1}{20}$	2.344×10^{-14}	6.677×10^{-5}
$\frac{1}{40}$	9.038×10^{-14}	1.644×10^{-5}
$\frac{1}{80}$	1.767×10^{-13}	4.068×10^{-6}
$\frac{1}{160}$	7.809×10^{-12}	1.014×10^{-6}

Table 2.6: $r = 2$

In order to study a case in which the exact solution did not belong to the discrete space $\boldsymbol{W}_h$, we decided to perform a final experiment with the same parameters and degree of the previous test but with the following solutions:

$$\boldsymbol{u}_{ex} = \left[\sin^2(y)\,,\, \cos^2(x)\right]^T\,, \quad p_{ex} = \sin(x)\cos(y)$$

and $\boldsymbol{f}$ deduced from these functions. As it can be seen in Figure 2.8 we achieved an order of two for both the unknowns, this result is in perfect agreement with the theory since both orders of convergence increased by one.

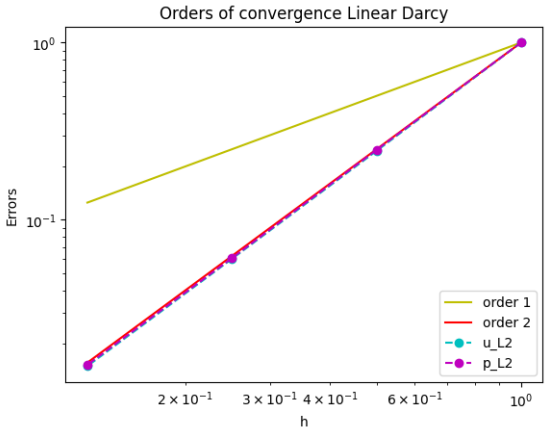

Figure 2.8: $r = 2$, trigonometric case

h	$\|\|\boldsymbol{u}_{ex} - \boldsymbol{u}_h\|\|_{L^2}$	$\|\|p_{ex} - p_h\|\|_{L^2}$
$\frac{1}{20}$	1.230×10^{-4}	4.602×10^{-5}
$\frac{1}{40}$	3.013×10^{-5}	1.141×10^{-5}
$\frac{1}{80}$	7.412×10^{-6}	2.799×10^{-6}
$\frac{1}{160}$	1.839×10^{-6}	6.993×10^{-7}

Table 2.7: $r = 2$, trigonometric case

For the details on the code we refer to the Python script named "STEP1-LinearDarcy", with this experiment we close the first chapter of our report.

Solving the problems in cascata

Once the study of the two sub-problems was completed, we moved on to the second step of our project, namely the resolution of the two systems in cascata. In this short section we took advantage of all the knowledge acquired in the previous chapter in order to use the velocity solution of problem (2.1) as advection velocity for problem (2.2), hence we solved these two systems one after the other:

$$\begin{cases} \nu \boldsymbol{u} + \nabla p = \boldsymbol{f} \ \text{ in } \ \Omega, \\ \operatorname{div} \boldsymbol{u} = 0 \ \text{ in } \ \Omega, \\ p = p_D \ \text{ on } \ \partial\Omega \end{cases} \qquad \begin{cases} -\kappa \Delta \theta + (\boldsymbol{u} \cdot \nabla)\theta = g \ \text{ in } \ \Omega, \\ \theta = \theta_0 \ \text{ on } \ \partial\Omega \end{cases}$$

The deductions of the weak formulations and the discrete approximations are exactly the same described in chapter one, in particular (2.18) for the transport-diffusion problem and (2.21 - 2.22) for the Darcy system. First, we had to pay attention at the regularity of $\boldsymbol{u}$, since in this setting the solution of the Darcy system also plays the role of convective velocity. We needed $\boldsymbol{u} \in \boldsymbol{H}(\operatorname{div}; \Omega)$, which is exactly what we get from the first problem. Second, we want to point out that we considered $\mathcal{T}_h$ as a conforming mesh of Ω, and it is used for the discretization of both the Darcy problem and the diffusion-transport problem. This choice is due to the fact that Raviart-Thomas elements need this type of mesh, even if dG method for diffusion-transport works also with more generic meshes. A possible further implementation could be using a dG method also for the Darcy problem.

3.1 Numerical experiment cascade problem

As in the previous experiments we performed a convergence test with the aim of inspecting the correct behaviour of our implementation. We merged the previous numerical implementations in a single function in order to solve both discrete formulations. Taking inspiration from the above data we set:

$$\Omega = (0,1) \times (0,1)\,, \quad \nu = 10\,, \quad \kappa = 5 \times 10^{-4}\,, \quad \boldsymbol{f} = [0,0]^T\,, \quad g = -4\kappa - \frac{4xy}{\nu}\,, \quad \alpha = 9.1\,,$$

with exact solutions:

$$\boldsymbol{u}_{ex} = \left[-\frac{1}{\nu} y\,, -\frac{1}{\nu} x \right]^T\,, \quad p_{ex} = xy\,, \quad \theta_{ex} = x^2 + y^2\,.$$

For the first experiment we chose the space of broken polynomials of order one and zero for the discrete space of temperature and pressure respectively, instead for the velocity of the fluid we chose the already mentioned Raviart-Thomas elements of order one. The results of the first experiment are reported in Figure 3.1 and Table 3.1.

h	$\|\|\theta_{ex} - \theta_h\|\|_{L^2}$	$\|\|\boldsymbol{u}_{ex} - \boldsymbol{u}_h\|\|_{L^2}$	$\|\|p_{ex} - p_h\|\|_{L^2}$
$\frac{1}{20}$	1.842×10^{-4}	2.041×10^{-3}	6.805×10^{-3}
$\frac{1}{40}$	4.628×10^{-5}	1.020×10^{-3}	3.402×10^{-3}
$\frac{1}{80}$	1.155×10^{-5}	5.103×10^{-4}	1.701×10^{-3}
$\frac{1}{160}$	2.876×10^{-6}	2.551×10^{-4}	8.505×10^{-4}

Table 3.1: $r = 1$

h	$\|\|\theta_{ex} - \theta_h\|\|_{L^2}$	$\|\|\boldsymbol{u}_{ex} - \boldsymbol{u}_h\|\|_{L^2}$	$\|\|p_{ex} - p_h\|\|_{L^2}$
$\frac{1}{20}$	1.147×10^{-7}	4.356×10^{-13}	4.166×10^{-5}
$\frac{1}{40}$	4.942×10^{-8}	2.069×10^{-12}	1.041×10^{-5}
$\frac{1}{80}$	1.943×10^{-8}	1.389×10^{-12}	2.604×10^{-6}
$\frac{1}{160}$	6.773×10^{-9}	1.822×10^{-12}	6.510×10^{-7}

Table 3.2: $r = 2$

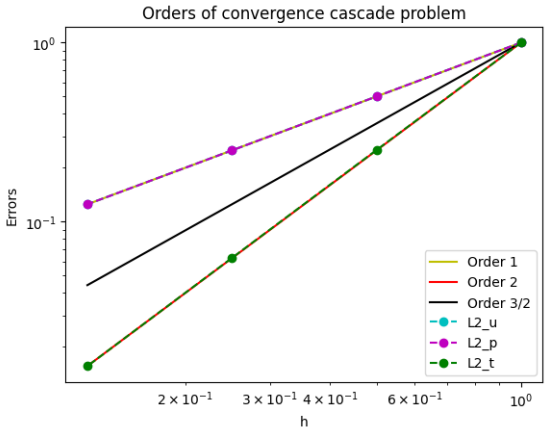

Figure 3.1: $r = 1$

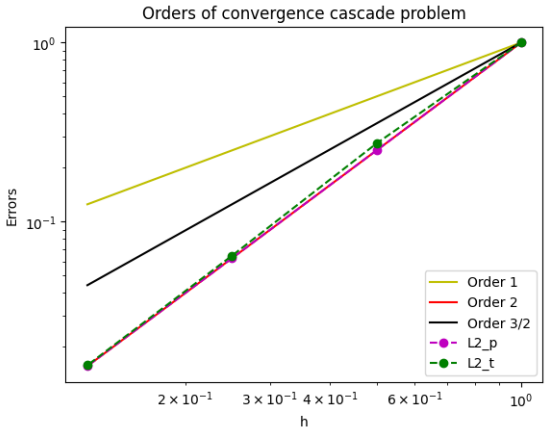

Figure 3.2: $r = 2$

We achieved an order of convergence equal to one for the L^2 norm of both velocity and pressure and an order equal to two for the L^2 norm of the temperature. These results match with the data obtained in the first chapter, hence they confirm the correct behaviour of our numerical scheme. We then decided to increase the degree of the discrete spaces by picking $r = 2$. In Figure 3.2 and Table 3.2 it can be seen the results. This second experiment confirm the behaviour of pressure and velocity: like the test of section **2.5** the pressure presents an order of convergence equal to 2 instead the velocity reaches the machine precision since also in this case $\boldsymbol{u}_{ex} \in \boldsymbol{W}_h$. For the same reason of the previous section, we did not represent the error for velocity in the plot of trends (Fig.3.2). Also for the L^2 norm of the temperature we achieved an order equal to two, consistently with the results of the first chapter.

As in section **2.5**, we decided to study also a case in which the exact solution does not belong to the discrete space of the trial functions, thus we implemented a test with trigonometric functions. We used the data presented below:

$$\boldsymbol{u}_{ex} = \left[\sin^2 y, \cos^2 x\right] , \quad p_{ex} = \sin x \cos y , \quad \theta_{ex} = \sin y \cos x ,$$

and the parameters set before. We obtained the following results:

h	$\|\|\theta_{ex} - \theta_h\|\|_{L^2}$	$\|\|\boldsymbol{u}_{ex} - \boldsymbol{u}_h\|\|_{L^2}$	$\|\|p_{ex} - p_h\|\|_{L^2}$
$\frac{1}{20}$	5.568×10^{-6}	1.056×10^{-4}	3.231×10^{-5}
$\frac{1}{40}$	5.013×10^{-7}	2.647×10^{-5}	8.045×10^{-6}
$\frac{1}{80}$	9.497×10^{-8}	6.626×10^{-6}	2.009×10^{-6}
$\frac{1}{160}$	2.841×10^{-8}	1.657×10^{-6}	5.028×10^{-7}

Table 3.3: $r = 2$, trigonometric case

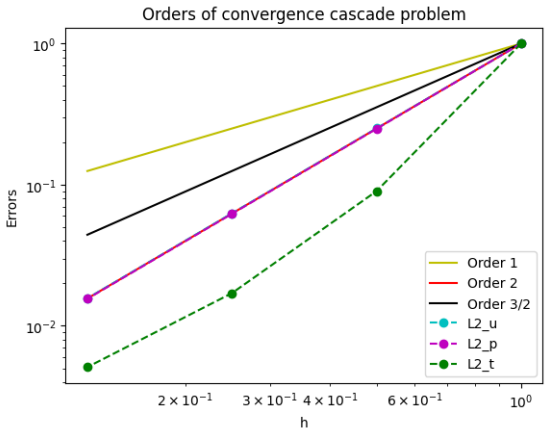

Figure 3.3: $r = 2$, trigonometric case

Consistently with the previous results, we achieved an order of convergence equal to two for both the L^2 norm of pressure and velocity. The temperature, like the other unknowns, presents an order of convergence that tends to two. For the details on the implementation we refer to the Python script named "STEP2-Cascata".

Remark: In the plots all the errors are rescaled with respect to the first one of the corresponding series, while in the tables there are the absolute errors.

Non-linear Problem

4.1 Weak formulation and discrete formulation

The main focus of this chapter was to find a way to treat the non-linearity appearing in the Darcy-Forchheimer problem:

$$\begin{cases} \nu \boldsymbol{u} + \beta |\boldsymbol{u}| \boldsymbol{u} + \nabla p = \boldsymbol{f} \quad \text{in } \Omega, \\ \operatorname{div} \boldsymbol{u} = 0\,, \quad \text{in } \Omega \\ p = p_D \quad \text{on } \partial\Omega \end{cases} \tag{4.1}$$

First of all we introduced the functional setting of the problem:

$$\boldsymbol{X} = \{\boldsymbol{u} \in [L^3(\Omega)]^d \ \text{ s.t. } \operatorname{div} \boldsymbol{u} \in L^2(\Omega)\}, \quad \|\boldsymbol{u}\|_X = \|\boldsymbol{u}\|_{L^3} + \|\operatorname{div}\boldsymbol{u}\|_{L^2}$$
$$M = L^2(\Omega), \quad \|p\|_M = \|p\|_{L^2}$$

The space $\boldsymbol{X}$ is similar to the space $\boldsymbol{H}(\operatorname{div};\Omega)$ (actually it is included in it) but with more regular functions, this choice is justified by the process that leads to the weak formulation; indeed, by exploiting the Holder inequality, we need a L^3-regularity in order to define the integral of the non-linear term. The space for the pressure instead is the usual $L^2(\Omega)$. Also for this problem we could choose Dirichlet boundary condition rather than a Neumann boundary condition. Accordingly with what we did in the previous problems, we considered a Dirichlet boundary condition for pressure. On the other hand, if we had imposed a Neumann condition in (4.1) e.g. $\boldsymbol{u} \cdot \boldsymbol{n} = \psi$, we would have taken the space $M = L^2_0(\Omega)$ moreover we should have to ensure the compatibility condition:

$$\int_{\partial\Omega} \psi \ d\sigma = 0\,.$$

as a consequence of the divergence theorem. The weak formulation reads:

$$\text{Find } (\boldsymbol{u}, p) \in \boldsymbol{X} \times M \ \text{ s.t.}$$

$$\begin{cases} \int_\Omega (\nu \boldsymbol{u} + \beta |\boldsymbol{u}| \boldsymbol{u}) \cdot \boldsymbol{v} - \int_\Omega p \operatorname{div} \boldsymbol{v} = \int_\Omega \boldsymbol{f} \cdot \boldsymbol{v} - \int_{\partial\Omega} p_D \boldsymbol{v} \cdot \boldsymbol{n} \qquad \forall \boldsymbol{v} \in \boldsymbol{X} \\ \int_\Omega q \operatorname{div} \boldsymbol{u} = 0 \qquad \forall q \in M \end{cases} \tag{4.2}$$

Where $\nu, \beta > 0$, $\boldsymbol{f} \in L^2(\Omega)$ and $p_D \in H^{1/2}(\partial\Omega)$. This problem is well-posed, we refer to [4] for existence, uniqueness and a-priori bounds (Theorem 3.3) and for the proof that the inf-sup condition is satisfied (Lemma 3.2). Then we introduced a conforming mesh $\mathcal{T}_h$ and we discretized the problem by using again Raviart-Thomas elements for velocity and piecewise polynomials for pressure, namely

$$\boldsymbol{X}_h = \{\boldsymbol{v}_h \in \boldsymbol{H}(\operatorname{div}; \mathcal{T}_h)\,, \ \ \boldsymbol{v}_h|_{\mathcal{K}} \in \mathbb{RT}^r(\mathcal{K})\,, \ \ \forall \mathcal{K} \in \mathcal{T}_h\}\,,$$

$$M_h = \mathbb{P}^{r-1}(\mathcal{T}_h)\,.$$

The discrete formulation reads:

$$\text{Find } (\boldsymbol{u}_h, p_h) \in \boldsymbol{X}_h \times M_h \ \text{ s.t.}$$

$$\begin{cases} \int_\Omega (\nu \boldsymbol{u}_h + \beta |\boldsymbol{u}_h| \boldsymbol{u}_h) \cdot \boldsymbol{v}_h - \int_\Omega p_h \operatorname{div} \boldsymbol{v}_h = \int_\Omega \boldsymbol{f} \cdot \boldsymbol{v}_h - \int_{\partial\Omega} p_D \boldsymbol{v}_h \cdot \boldsymbol{n} \qquad \forall \boldsymbol{v}_h \in \boldsymbol{X}_h \\ \int_\Omega q_h \operatorname{div} \mathbf{u}_h = 0 \qquad \forall q_h \in M_h \end{cases} \tag{4.3}$$

We refer again to [4] for the well-posedness of the discrete problem (Theorem 3.5) and the correspondent proof for the discrete inf-sup condition (Lemma 3.4).

4.2 Iterative linearization algorithm

In order to treat the non linearity we used a fixed point method to linearize the problem. We defined the operator that, given the data, solves the non linear problem:

$$F : (\nu, \beta, \boldsymbol{f}, p_D) \to (\boldsymbol{u}, p)$$

Since the solution depends also on the euclidean norm of $\boldsymbol{u}$ we rephrased this operator into

$$\tilde{F} : (\nu, \beta, \boldsymbol{f}, p_D, |\mathbf{u}|) \to (\boldsymbol{u}, p)$$

From this we deduced the fixed point structure: given some initial condition $\boldsymbol{u}^0$, p^0: for $k > 0$

$$(\boldsymbol{u}_h^{k+1}, p_h^{k+1}) = \tilde{F}(\nu, \beta, \boldsymbol{f}, p_D, |\boldsymbol{u}_h^k|) \tag{4.4}$$

The initial conditions are the solution of a linear Darcy problem with the same physical coefficients. Then the algorithm reads:

$$\text{Given } \ \boldsymbol{u}^0, p^0, \ \ \forall k > 0 \ \text{ find } \ (\boldsymbol{u}_h^{k+1}, p_h^{k+1}) \in \boldsymbol{X}_h \times M_h \ \text{ s.t.}$$

$$\begin{cases} \int_\Omega (\nu + \beta|\boldsymbol{u}_h^k|)\ \boldsymbol{u}_h^{k+1} \cdot \boldsymbol{v}_h - \int_\Omega p_h^{k+1} \mathrm{div} \boldsymbol{v}_h = \int_\Omega \boldsymbol{f} \cdot \boldsymbol{v}_h - \int_{\partial\Omega} p_D \boldsymbol{v}_h \cdot \boldsymbol{n} & \forall \boldsymbol{v}_h \in \boldsymbol{X}_h \\ \int_\Omega q_h \mathrm{div} \mathbf{u}_h^{k+1} = 0 & \forall q_h \in M_h \end{cases} \tag{4.5}$$

The formulation above is a linear Darcy problem with a viscosity coefficient that varies at every iteration. It takes into account the quantity $\beta|\boldsymbol{u}_h^k|$ as an additive viscosity coefficient to the true physical viscosity of the problem. It is important to point out that at every iteration we solve a well-posed problem and also that the algorithm is consistent, indeed if we replace the exact solution in the scheme we have convergence in one iteration. We then rewrote the problem in its algebraic form. We introduced two basis for the discrete spaces $\boldsymbol{X}_h = \mathrm{span}\{\boldsymbol{\phi}_i\}$ and $M_h = \mathrm{span}\{\psi_i\}$ and then we rewrote the unknowns $\boldsymbol{u}_h\,, p_h$ as linear combination of elements of the basis:

$$\boldsymbol{u}_h = \sum_{i=1}^{m_1} \tilde{u}_i \boldsymbol{\phi}_i\,, \quad p_h = \sum_{i=1}^{m_2} \tilde{p}_i \psi_i$$

where with m_1, m_2 we refer to the dimension of the spaces and by $\tilde{u}_i$, $\tilde{p}_i$ the coefficients of the linear combinations. Then, by using the same notation as in [4], we introduced the functional matrices $D^{-1}(w)$, B its transpose B^T and G respectively corresponding to:

$$\left[D^{-1}(w)\right]_{i,j} = \int_\Omega (\nu + \beta|w|)\ \boldsymbol{\phi}_j \cdot \boldsymbol{\phi}_i\,, \qquad [B]_{i,j} = -\int_\Omega q_h \mathrm{div}\, \boldsymbol{u}_h\,, \qquad [G]_i = -\int_{\partial\Omega} p_D \boldsymbol{\phi}_i \cdot \boldsymbol{n} + \int_\Omega \boldsymbol{f} \cdot \boldsymbol{\phi}_i$$

Thanks to these definitions the iterative algorithm can be rephrased in algebraic form. The solutions $(\boldsymbol{u}_h^{k+1}, p_h^{k+1})$ are the result of a linear system for each iterations k:

$$\text{Given } \ \tilde{u}^0 \in \mathbb{R}^{m_1}\,,\ \tilde{p}^0 \in \mathbb{R}^{m_2}\,, \ \text{ Find } \ \tilde{u}^{k+1} \in \mathbb{R}^{m_1}\,,\ \tilde{p}^{k+1} \in \mathbb{R}^{m_2} \ \text{ s.t. :}$$

$$\begin{pmatrix} D^{-1}(\tilde{u}^k) & B \\ B^T & O \end{pmatrix} \begin{pmatrix} \tilde{u}^{k+1} \\ \tilde{p}^{k+1} \end{pmatrix} = \begin{pmatrix} G \\ O \end{pmatrix}$$

Even if we decrease the mathematical complexity by solving linear problems at every iteration, we have a considerable computational load since the matrix D^{-1} has to be computed at every iteration. For the problem of this section we checked numerically the convergence behaviour and we studied the robustness of the iterative algorithm.

4.3 Numerical experiment on the iterative algorithm

In this section we reported all the results obtained from the fixed point algorithm. Like all the previous implementation we introduced a mesh $\mathcal{T}_h$ and we set our domain Ω as the unit square $(0,1) \times (0,1)$. The converging metric to be inspected at every iteration is the error between two consecutive iterations, namely:

$$E = \frac{\|\boldsymbol{u}_h^k - \boldsymbol{u}_h^{k-1}\|_{\boldsymbol{H}(\mathrm{div};\Omega)}}{\|\boldsymbol{u}_h^k\|_{\boldsymbol{H}(\mathrm{div};\Omega)}} + \frac{\|p_h^k - p_h^{k-1}\|_{L^2(\Omega)}}{\|p_h^k\|_{L^2(\Omega)}}$$

The algorithm stops if this quantity is below a desired tolerance. Otherwise it goes on until a maximum number of iteration is reached. The aim of this experiment was to test the implementation of (4.5) with different values for the parameter β in order to understand how these change affects the errors and the number of the iterations needed for convergence. We recall that β it is the parameter that decides the "amount of non-linearity" in the problem, hence by changing it one can heavily influence the behaviour of the algorithm. In order to compare the results we fixed the refinement of the mesh to $h = \frac{1}{100}$, the tolerance of the fixed point loop to 1×10^{-8} and the number of maximum iterations to converge at 1000. The data used for the experiments are the following:

$$\nu = 10\,, \quad \boldsymbol{f} = \left[-\frac{\beta\, y}{\nu^2}\sqrt{x^2+y^2}\,, -\frac{\beta\, x}{\nu^2}\sqrt{x^2+y^2}\right]^T, \quad p_{ex} = xy\,, \quad \boldsymbol{u}_{ex} = \left[-\frac{y}{\nu}\,, -\frac{x}{\nu}\right]^T$$

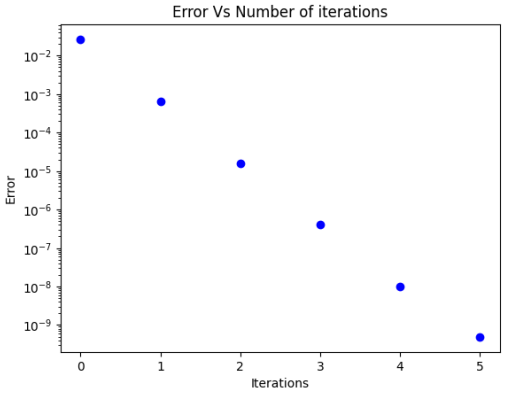

(a) $\beta = 0.1$, converge in 5 iterations

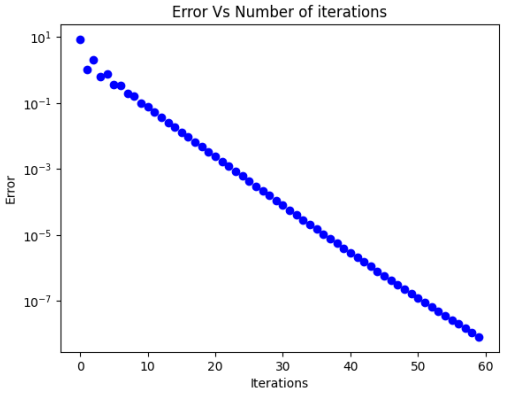

(b) $\beta = 10$, converge in 59 iterations

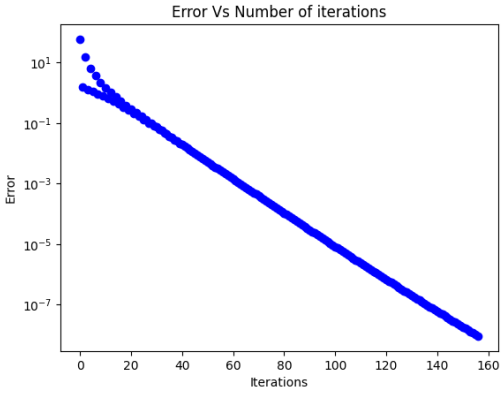

(c) $\beta = 30$, converge in 156 iterations

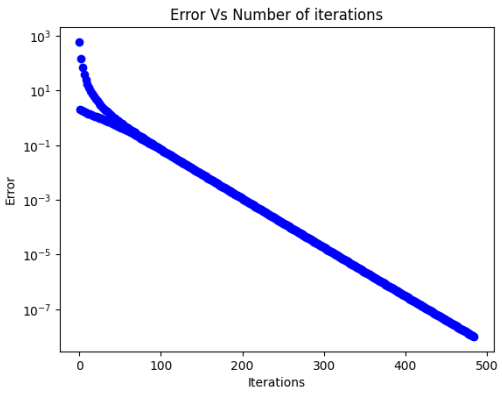

(d) $\beta = 100$, converge in 484 iterations

Figure 4.1: Graphs that display the trend of the error and the number of iterations for different values of β. On the x-axis we have the number of the iterations, instead on the y-axis the base 10 logarithm of the error defined in this section.

As expected from the theory high β values correspond to a larger number of iterations for convergence. This agrees with what we said before. Hence, as can be seen in the plots above, we needed more computations (thus more iterations) for problems with a more marked non-linear component. Another interesting feature of the algorithm is the initial oscillation of the error. Also in this case we can note a more marked presence of the behaviour for larger values of β. This is due to the fact that it is more difficult to approximate less linear functions, especially in the early iterations. Despite that, the algorithm is very robust and can successfully bear different values of the parameter. However, this experiment goes further than the true intent of the final implementation since for the actual applications in which we are interested the values of β do not go beyond 10. Lastly we were interested in understanding the relationship between the number of iterations and the different values attributed to β, hence we plotted this final graph:

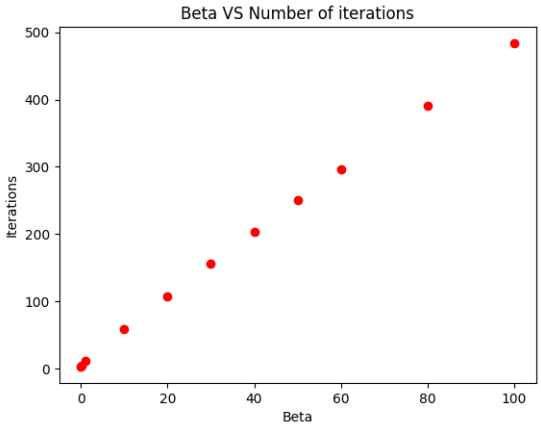

Figure 4.2: β vs number of iterations

As the reader can see the number of iterations is almost linearly dependent with respect to the parameter β. For the details on the implementation we refer to the Python script named "STEP3-Forchheimer-Problem".

Coupled Problem

The final step wraps up all the previous stages and focuses on the complete, fully coupled problem

$$\begin{cases} \nu(\theta)\boldsymbol{u} + \beta|\boldsymbol{u}|\boldsymbol{u} + \nabla p = \boldsymbol{f} \ \text{ in } \ \Omega, \\ \operatorname{div} \boldsymbol{u} = 0 \ \text{ in } \ \Omega, \\ -\kappa\Delta\theta + (\boldsymbol{u}\cdot\nabla)\theta = g \ \text{ in } \ \Omega, \\ p = p_D, \quad \theta = \theta_0 \ \text{ on } \ \partial\Omega \end{cases} \tag{5.1}$$

where $g \in L^2(\Omega),\ \theta_0 \in H^{1/2}(\Omega),\ \boldsymbol{f} \in [L^2(\Omega)]^d,\ p_D \in H^{1/2}(\partial\Omega)$ and $\nu : \mathbb{R} \to \mathbb{R}^+$ is a bounded $\mathcal{C}^1(\mathbb{R}^+)$, globally Lipschitz function, such that $0 < \nu_0 \le \nu(s) \le \nu_1$ for some $\nu_0,\ \nu_1 \in \mathbb{R}^+$. For the analysis we considered a generic function $\nu(\theta)$, while for the implementation we selected the particular model function $\nu(s) = 1 + e^{-s}$ as in [1].

5.1 Weak formulation and discrete formulation

We considered $\boldsymbol{X}$ and M defined as in the previous chapter and $V = H^1(\Omega)$. The weak formulation of the problem reads:

$$\text{Find } \ (\boldsymbol{u}, p, \theta) \in \boldsymbol{X} \times M \times V \ \text{ s.t. } \ \theta = \theta_0 \ \text{ and}$$

$$\begin{cases} \int_\Omega (\nu(\theta)\boldsymbol{u} + \beta|\boldsymbol{u}|\boldsymbol{u})\cdot\boldsymbol{v} - \int_\Omega p\operatorname{div}\boldsymbol{v} = \int_\Omega \boldsymbol{f}\cdot\boldsymbol{v} - \int_{\partial\Omega} p_D\boldsymbol{v}\cdot\boldsymbol{n} \qquad \forall \boldsymbol{v} \in \boldsymbol{X} \\ \int_\Omega q\operatorname{div}\boldsymbol{u} = 0 \qquad \forall q \in M \\ \kappa\int_\Omega \nabla\theta\cdot\nabla\rho + \int_\Omega (\boldsymbol{u}\cdot\nabla)\theta\rho = \int_\Omega g\rho \qquad \forall \rho \in V \end{cases} \tag{5.2}$$

This problem is well-posed under the assumptions on ν mentioned above. For the analysis it can be used the same argument as in [1] (Section 2.3) where the autors treat a very similar formulation of the problem. The idea is to find some a-priori bounds for the unknowns, then use the Galerkin method coupled with the Brouwer's fixed point method and find a solution as a limit for the subsequencies. Also for the discrete problem we considered $\boldsymbol{X}_h,\ M_h$ as in the previous chapter and $V_h = \mathbb{P}^n(\mathcal{T}_h)$. Since the velocity is an unknown we had to redefine the bilinear form b_h as

$$b_h(\,\cdot\,,\,\cdot\,,\,\cdot\,) : \boldsymbol{X}_h \times V_h \times V_h \to \mathbb{R}$$

The skew-symmetry of the form is preserved, indeed we have that $b_h(\boldsymbol{u}_h, \theta_h, \theta_h) = 0$. The discrete problem reads:

$$\text{Find } \ (\boldsymbol{u}_h, p_h, \theta_h) \in \boldsymbol{X}_h \times M_h \times V_h \ \text{ s.t.}$$

$$\begin{cases} \int_\Omega (\nu(\theta_h)\boldsymbol{u}_h + \beta|\boldsymbol{u}_h|\boldsymbol{u}_h)\cdot\boldsymbol{v}_h - \int_\Omega p_h\operatorname{div}\boldsymbol{v}_h = \int_\Omega \boldsymbol{f}\cdot\boldsymbol{v}_h - \int_{\partial\Omega} p_D\boldsymbol{v}_h\cdot\boldsymbol{n} \qquad \forall \boldsymbol{v}_h \in \boldsymbol{X}_h \\ \int_\Omega q_h\operatorname{div}\boldsymbol{u}_h = 0 \qquad \forall q_h \in M_h \\ a_h(\theta_h, \rho_h) + b_h(\boldsymbol{u}_h, \theta_h, \rho_h) = l_h(\rho_h) \qquad \forall \rho_h \in V_h \end{cases} \tag{5.3}$$

where a_h and l_h are exactly (2.6) and (2.8) respectively. We then proceeded to find some a-priori bounds for the discrete solutions. This result can be used to prove existence and uniqueness for the discrete formulation.

Proposition 3. *There exist constants C_1, C_2 such that:*

$$\|\boldsymbol{u}_h\|_{\boldsymbol{X}} \le C_1 \left(\|\boldsymbol{f}\|^2_{L^2(\Omega)} + \|p_D\|^2_{H^{\frac{1}{2}}(\partial\Omega)} \right)^{1/3} \tag{5.4}$$

$$\|p_h\|_{L^2(\Omega)} \le C_2 \ \left(\|\boldsymbol{f}\|^2_{L^2(\Omega)} + \|p_D\|^2_{H^{1/2}(\partial\Omega)} \right)^{1/3} \tag{5.5}$$

and if $\theta_0 \in L^\infty(\partial\Omega)$ there exist C_3 s.t.

$$\|\theta_h\|_{DG} \le C_3 \left(\|g\|_{L^2(\Omega)} + \|\theta_0\|_{L^2(\mathcal{F}_h)} + \|\theta_0\|^{3/2}_{L^\infty(\partial\Omega)} + \|\boldsymbol{f}\|^2_{L^2(\Omega)} + \|p_D\|^2_{H^{1/2}(\partial\Omega)} \right) \tag{5.6}$$

Proof. Take $(\boldsymbol{v}_h, q_h) = (\boldsymbol{u}_h, p_h)$ in the first equation of (5.3), thanks to the assumptions on $\nu(\theta)$ we can write

$$\nu_0 \int_\Omega |\boldsymbol{u}_h|^2 \ + \beta \int_\Omega |\boldsymbol{u}_h|^3 \leq \int_\Omega \boldsymbol{f} \cdot \boldsymbol{u}_h \ - \int_{\partial\Omega} p_D \boldsymbol{u}_h \cdot \boldsymbol{n}$$

$\boldsymbol{u}_h \in \boldsymbol{X} \subset \boldsymbol{H}(\mathrm{div}, \Omega)$ so we can apply the normal trace operator $\gamma_\nu : \boldsymbol{H}(\mathrm{div}, \Omega) \to H^{-\frac{1}{2}}(\partial\Omega)$, from which $\gamma_\nu(\boldsymbol{u}_h) = \boldsymbol{u}_h \cdot \boldsymbol{n}|_{\partial\Omega} \in H^{-\frac{1}{2}}(\partial\Omega)$. Since $p_D \in H^{\frac{1}{2}}(\partial\Omega)$ we can rewrite the right hand side as

$$\nu_0 \int_\Omega |\boldsymbol{u}_h|^2 \ + \beta \int_\Omega |\boldsymbol{u}_h|^3 \leq \int_\Omega \boldsymbol{f} \cdot \boldsymbol{u}_h \ - < \boldsymbol{u}_h \cdot \boldsymbol{n}, p_D >$$

where the duality is well defined thanks to the assumptions on the regularity. In the right hand side, for the first term we use Cauchy-Schwarz's inequality and Young's inequality to separate the datum from the unknown, while for the second term we use the continuity of the normal trace of $\boldsymbol{u}_h$ seen as an element of $H^{-\frac{1}{2}}$ and Young's inequality as well

$$\nu_0 \|\boldsymbol{u}_h\|^2_{L^2(\Omega)} \ + \beta \|\boldsymbol{u}_h\|^3_{L^3(\Omega)} \leq \frac{\nu_0}{4} \|\boldsymbol{u}_h\|^2_{L^2(\Omega)} + \frac{1}{\nu_0} \|\boldsymbol{f}\|^2_{L^2(\Omega)} + \frac{\nu_0}{4} \|\boldsymbol{u}_h \cdot \boldsymbol{n}\|^2_{H^{-1/2}(\partial\Omega)} + \frac{1}{\nu_0} \|p_D\|^2_{H^{1/2}(\partial\Omega)}$$

We can exploit the continuity of the normal trace operator to get

$$\nu_0 \|\boldsymbol{u}_h\|^2_{L^2(\Omega)} + \beta \|\boldsymbol{u}_h\|^3_{L^3(\Omega)} \leq \frac{\nu_0}{4} \|\boldsymbol{u}_h\|^2_{L^2(\Omega)} + \frac{1}{\nu_0} \|\boldsymbol{f}\|^2_{L^2(\Omega)} + \frac{\nu_0}{4} \|\boldsymbol{u}_h\|^2_{\boldsymbol{H}(\mathrm{div},\Omega)} + \frac{1}{\nu_0} \|p_D\|^2_{H^{\frac{1}{2}}(\partial\Omega)} \tag{5.7}$$

Now if we take $(\boldsymbol{v}_h, q_h) = (0, -\mathrm{div}\ \boldsymbol{u}_h)$ we get

$$\|\mathrm{div}\ \boldsymbol{u}_h\|^2_{L^2(\Omega)} \leq 0 \tag{5.8}$$

If we combine (5.7) and (5.8) we get (5.4)

$$\|\boldsymbol{u}_h\|_{\boldsymbol{X}} \leq C_1 \left(\|\boldsymbol{f}\|^2_{L^2(\Omega)} + \|p_D\|^2_{H^{\frac{1}{2}}(\partial\Omega)} \right)^{1/3}$$

In order to find an estimate for pressure we exploit the inf-sup condition that holds for the Darcy-Forchheimer problem (see [4], Lemma 3.4), we call γ the constant of the condition.

$$\begin{aligned} \|p_h\|_{L^2(\Omega)} &\leq \frac{1}{\gamma} \sup_{v_h \in V_h} \frac{(p_h, \mathrm{div}\ \boldsymbol{v}_h)}{\|\boldsymbol{v}_h\|_X} \\ &= \frac{1}{\gamma} \sup_{v_h \in V_h} \frac{(\nu(\theta_h)\boldsymbol{u}_h, \boldsymbol{v}_h) + \beta(|\boldsymbol{u}_h|\boldsymbol{u}_h, \boldsymbol{v}_h) - (\boldsymbol{f}, \boldsymbol{v}_h) + < \boldsymbol{v}_h \cdot \boldsymbol{n}, p_D >}{\|\boldsymbol{v}_h\|_X} \end{aligned}$$

Now we apply the Holder inequality on the first three terms and continuity on the last term

$$\begin{aligned} \|p_h\|_{L^2(\Omega)} &\leq \frac{1}{\gamma} \ \frac{\nu_1 \|\boldsymbol{u}_h\|_{L^2} \|\boldsymbol{v}_h\|_{L^2} + \beta \| \ |\boldsymbol{u}_h| \boldsymbol{u}_h\|_{L^{3/2}} \|\boldsymbol{v}_h\|_{L^3} + \|\boldsymbol{f}\|_{L^2} \|\boldsymbol{v}_h\|_{L^2} + \|\boldsymbol{v}_h\|_{\boldsymbol{H}(\mathrm{div},\Omega)} \|p_D\|_{L^2(\partial\Omega)}}{\|\boldsymbol{v}_h\|_{\boldsymbol{X}}} \\ &\leq C_2 \ \left(\|\boldsymbol{f}\|^2_{L^2(\Omega)} + \|p_D\|^2_{H^{1/2}(\partial\Omega)} \right)^{1/3} \end{aligned}$$

which is (5.5). The estimate for θ_h exploits the skew-symmetry of b_h and the coercivity of a_h. Moreover, we assume a more restrictive regularity on the boundary data, namely $\theta_0 \in L^\infty(\partial\Omega)$. This assumption is physically possible, indeed it makes sense that the temperature does not increase indefinitely. For this reason we take a bounded quantity (up to set of zero measure). If we take $\rho = \theta_h$

$$\begin{aligned} \|\theta_h\|^2_{DG} \leq a_h(\theta_h, \theta_h) &= a_h(\theta_h, \theta_h) + b_h(\theta_h, \theta_h) = l_h(\theta_h) \\ &= \int_\Omega g\theta_h \ - \sum_{F \in \mathcal{F}_h^B} \int_F \kappa \nabla_h \theta_h \cdot \boldsymbol{n} \theta_0 \ + \sum_{F \in \mathcal{F}_h^B} \int_F \theta_0 \theta_h \gamma \ - \frac{1}{2} \sum_{F \in \mathcal{F}_h^B} \int_F \boldsymbol{u_h} \cdot \boldsymbol{n}\, \theta_0 \theta_h \\ &\leq \|g\|_{L^2} \|\theta_h\|_{L^2} + C \|\nabla_h \theta_h\|_{L^2} \left(\sum_{F \in \mathcal{F}_h} \frac{1}{h_F} \| \ [\![\theta_0]\!] \ \|^2_{L^2} \right)^{1/2} + \\ &\quad + \gamma \|\theta_0\|_{L^2(\mathcal{F}_h)} \|\theta_h\|_{L^2(\mathcal{F}_h)} + \frac{1}{2} \|\boldsymbol{u}_h\|_{\boldsymbol{H}(\mathrm{div},\Omega)} \|\theta_0\|_{L^\infty(\partial\Omega)} \|\theta_h\|_{L^2(\mathcal{F}_h)} \end{aligned}$$

To get the latter we exploit the following estimate from [3] (Lemma 4.11) for the second sum of integrals: $\forall v_h, w_h \in V_h$

$$\left| \sum_{F \in \mathcal{F}_h} \int_F \{\!\{\nabla_h v_h\}\!\} \cdot \boldsymbol{n} \, [\![w_h]\!] \right| \leq C_{tr} \|\nabla_h v_h\|_{L^2(\Omega)} \left(\sum_{F \in \mathcal{F}_h} \frac{1}{h_F} \| \, [\![w_h]\!] \, \|^2_{L^2} \right)^{1/2}$$

Where C_{tr} is the trace constant and is independent from h. Now the L^2-norm can be increased by the DG-norm (see [6]) and both the L^2-norm of the gradient and the skeleton norm can be increased by the DG-norm too. We have that

$$\|\theta_h\|^2_{DG} \leq \left(\|g\|_{L^2} + C \left(\sum_{F \in \mathcal{F}_h} \frac{1}{h_F} \| \, [\![\theta_0]\!] \, \|^2_{L^2} \right)^{1/2} + \gamma \|\theta_0\|_{L^2(\mathcal{F}_h)} + \frac{1}{2} \|\boldsymbol{u}_h\|_X \|\theta_0\|_{L^\infty(\partial\Omega)} \right) \|\theta_h\|_{DG}$$

Now we use Young inequality and we get

$$\|\theta_h\|_{DG} \leq C_3 \left(\|g\|_{L^2} + \|\theta_0\|_{L^2(\mathcal{F}_h)} + \|\theta_0\|^{3/2}_{L^\infty(\partial\Omega)} + \|\boldsymbol{f}\|^2_{L^2(\Omega)} + \|p_D\|^2_{H^{1/2}(\partial\Omega)} \right) \tag{5.9}$$

which is (5.6).

□

5.2 Iterative linearization algorithm

Also for this problem we exploited a fixed point technique in order to treat the non linearity and the coupling between the equations. The philosophy is the same of the previous step. We considered the operator

$$F : (\nu(\cdot), \beta, \boldsymbol{f}, \kappa, g, \theta_0, p_D) \to (\boldsymbol{u}, p, \theta) \tag{5.10}$$

and as before we rephrased this into a fixed point structure like

$$\tilde{F} : (\nu(\cdot), \beta, \boldsymbol{f}, \kappa, g, \theta_0, p_D, \boldsymbol{u}_h^k, \theta_h^k) \to (\boldsymbol{u}_h^{k+1}, p_h^{k+1}, \theta_h^{k+1}) \tag{5.11}$$

The algorithm we present is:

$$\text{Given } (\boldsymbol{u}_h^0, p_h^0, \theta_h^0), \text{ for } k > 0 \text{ find } (\boldsymbol{u}_h^{k+1}, p_h^{k+1}, \theta_h^{k+1}) \in \boldsymbol{X}_h \times M_h \times V_h \quad \text{s.t.}$$

$$\begin{cases} \int_\Omega (\nu(\theta_h^k) + \beta |\boldsymbol{u}_h^k|) \, \boldsymbol{u}_h^{k+1} \cdot \boldsymbol{v}_h - \int_\Omega p_h^{k+1} \text{div} \boldsymbol{v}_h = \int_\Omega \boldsymbol{f} \cdot \boldsymbol{v}_h - \int_{\partial\Omega} p_D \boldsymbol{v}_h \cdot \boldsymbol{n} & \forall \boldsymbol{v}_h \in \boldsymbol{X}_h \\ \int_\Omega q_h \text{ div } \boldsymbol{u}_h^{k+1} = 0 & \forall q_h \in M_h \\ a_h(\theta_h^{k+1}, \rho_h) + b_h(\theta_h^{k+1}, \rho_h) = l_h(\rho_h) & \forall \rho_h \in V_h \end{cases} \tag{5.12}$$

At every iteration we solve a problem like the one from chapter **3**, namely a linear Darcy problem in cascata with the diffusion-transport equation. Here the viscosity coefficient takes into account also the value of the temperature at the previous iteration. It is important to note that the non-linearity from the Forchheimer term and the coupling created by $\nu(\theta)$ are treated simultaneously, meaning that the linearization technique we used involves at every iteration both the non linear term and the coefficient ν, leading to a linear problem to solve.

The algorithm is consistent, indeed if you replace $(\boldsymbol{u}_h, p_h, \theta_h)$ inside the scheme we get exactly the discrete formulation of the problem and the convergence is in 1 iteration. We then investigate the convergence of the scheme.

Proposition 4. *Let C be the coercivity constant of a_h and L the Lipschitz constant of $\nu(s)$. If*

$$\textit{(i)} \ \theta_h^k \in L^\infty(\Omega) \ \forall k, \wedge \sup_{k \geq 0} \|\theta_h^k\|_{L^\infty} < M_\theta < \infty$$

$$\textit{(ii)} \ \boldsymbol{u}_h^k \in [L^\infty(\Omega)]^d \ \forall k, \wedge \sup_{k \geq 0} \|\boldsymbol{u}_h^k\|_{L^\infty} < M_u < \infty$$

$$\textit{(iii)} \left(1 + M_\theta \tfrac{1}{C\sqrt{\nu_0}} \ \tfrac{5}{2}\right) \ M_u \ \max\{L, \beta\} < 1$$

then the algorithm (5.12) converges as $k \to \infty$.

Proof. Let us consider $(\boldsymbol{u}_h^{k+1}, p_h^{k+1}, \theta_h^{k+1})$ and $(\boldsymbol{u}_h^k, p_h^k, \theta_h^k)$ solutions of two consecutive iterations. Let us define

$$\begin{aligned} \boldsymbol{e}_u^k &:= \boldsymbol{u}_h^{k+1} - \boldsymbol{u}_h^k \\ e_p^k &:= p_h^{k+1} - p_h^k \\ e_\theta^k &:= \theta_h^{k+1} - \theta_h^k \end{aligned}$$

These are the errors between two consecutive iterations. Now we consider the difference between the two problems solved in the iterations k and $k+1$, and we obtain

$$\begin{cases} \int_\Omega \left[(\nu(\theta_h^k) + \beta|\boldsymbol{u}_h^k|)\ \boldsymbol{u}_h^{k+1} - (\nu(\theta_h^{k-1}) + \beta|\boldsymbol{u}_h^{k-1}|)\ \boldsymbol{u}_h^k\right] \cdot \boldsymbol{v}_h - \int_\Omega (p_h^{k+1} - p_h^k) \mathrm{div} \boldsymbol{v}_h = 0 \qquad \forall \boldsymbol{v}_h \in \boldsymbol{X}_h \\ \int_\Omega q_h\ \mathrm{div}\ (\boldsymbol{u}_h^{k+1} - \boldsymbol{u}_h^k) = 0 \qquad \forall q_h \in M_h \\ a_h(\theta_h^{k+1} - \theta_h^k, \rho_h) + b_h(\boldsymbol{u}_h^{k+1}, \theta_h^{k+1}, \rho_h) - b_h(\boldsymbol{u}_h^k, \theta_h^k, \rho_h) = 0 \qquad \forall \rho_h \in V_h \end{cases} \tag{5.13}$$

In the first equation we add $\pm(\nu(\theta_h^k) + \beta|\boldsymbol{u}_h^k|)\ \boldsymbol{u}_h^k$. The last equation is not linear in both velocity and temperature so we need to add $\pm\ b_h(\boldsymbol{u}_h^{k+1}, \theta_h^k, \rho_h)$. Our goal is to have a problem where the errors are the unknowns. Since the right hand sides are equal for the two problems, the one for the errors has homogeneous equations:

$$\begin{cases} \int_\Omega (\nu(\theta_h^k) + \beta|\boldsymbol{u}_h^k|)\ \boldsymbol{e}_u^k \cdot \boldsymbol{v}_h - \int_\Omega e_p^k\ \mathrm{div} \boldsymbol{v}_h = \int_\Omega (\nu(\theta_h^{k-1}) - \nu(\theta_h^k) + \beta|\boldsymbol{u}_h^{k-1}| - \beta|\boldsymbol{u}_h^k|)\ \boldsymbol{u}_h^k \cdot \boldsymbol{v}_h \qquad \forall \boldsymbol{v}_h \in \boldsymbol{X}_h \\ \int_\Omega q_h\ \mathrm{div}\ \boldsymbol{e}_u^k = 0 \qquad \forall q_h \in M_h \\ a_h(e_\theta^k, \rho_h) + b_h(\boldsymbol{u}_h^{k+1}, e_\theta^k, \rho_h) + b_h(\boldsymbol{e}_u^k, \theta_h^k, \rho_h) = 0 \qquad \forall \rho_h \in V_h \end{cases} \tag{5.14}$$

Now we take $(\boldsymbol{v}_h, q_h, \rho_h) = (\boldsymbol{e}_u^k, e_p^k, e_\theta^k)$, we can do it since they are elements in the respective spaces. We use Cauchy-Schwartz inequality in the first equation

$$\|\sqrt{\nu_0}\ \boldsymbol{e}_u^k\|_{L^2}^2 \leq \|(\nu(\theta_h^{k-1}) - \nu(\theta_h^k) + \beta|\boldsymbol{u}_h^{k-1}| - \beta|\boldsymbol{u}_h^k|)\ \boldsymbol{u}_h^k \sqrt{\nu_0}\|_{L^2}\ \|\sqrt{\nu_0}\boldsymbol{e}_u^k\|_{L^2} \tag{5.15}$$

Now we repeat it but taking $(\boldsymbol{v}_h, q_h, \rho_h) = (0, -\sqrt{\nu_0}\ \mathrm{div}\boldsymbol{e}_u^k, e_\theta^k)$. Adding together the first and second equations in (5.14) we get

$$\|\sqrt{\nu_0}\ \mathrm{div}\ \boldsymbol{e}_u^k\|_{L^2}^2 \leq 0 \tag{5.16}$$

If we combine the first equation in (5.15) and (5.16) and we consider the advection-diffusion equation too, we get

$$\begin{cases} \|\sqrt{\nu_0}\ \boldsymbol{e}_u^k\|_{\boldsymbol{H}(\mathrm{div},\Omega)}^2 \leq \|(\nu(\theta_h^{k-1}) - \nu(\theta_h^k) + \beta|\boldsymbol{u}_h^{k-1}| - \beta|\boldsymbol{u}_h^k|)\ \boldsymbol{u}_h^k \sqrt{\nu_0}\|_{L^2}\ \|\sqrt{\nu_0}\boldsymbol{e}_u^k\|_{\boldsymbol{H}(\mathrm{div},\Omega)} \\ a_h(e_\theta^k, e_\theta^k) + b_h(\boldsymbol{u}_h^{k+1}, e_\theta^k, e_\theta^k) = -\ b_h(\boldsymbol{e}_u^k, \theta_h^k, e_\theta^k) \end{cases} \tag{5.17}$$

In the first equation we simplify by the $\boldsymbol{H}(\mathrm{div})$-norm. In the second equation we exploit the skew-symmetry of b_h, hence the second term in the left hand side is null. We assume that $\theta_h^k \in L^\infty(\Omega)$, $\forall k$ which is physically possible as we pointed out in proposition 3. Then, let C the coercivity constant of a_h:

$$\begin{aligned} C\|e_\theta^k\|_{DG}^2 \leq a_h(e_\theta^k, e_\theta^k) &= -\ b_h(\boldsymbol{e}_u^k, \theta_h^k, e_\theta^k) \\ &\leq \|\theta_h^k\|_{L^\infty}\|\boldsymbol{e}_u^k\|_{L^2}\|\nabla_h e_\theta^k\|_{L^2} + \|\theta_h^k\|_{L^\infty}\left(\sum_{F\in\mathcal{F}_h^I} \|\ [[e_\theta^k]]\ \|_{L^2}^2\right)^{1/2}\left(\sum_{F\in\mathcal{F}_h^I} \|\ \{\{\boldsymbol{e}_u^k\}\}\ \|_{L^2}^2\right)^{1/2} \\ &+ \frac{1}{2}\|\theta_h^k\|_{L^\infty}\ \|e_\theta^k\|_{L^2}\ \|\boldsymbol{e}_u^k\|_{\boldsymbol{H}(\mathrm{div})} + \frac{1}{2}\|\theta_h^k\|_{L^\infty}\|e_\theta^k\|_{L^2}\|\ \mathrm{div}\ \boldsymbol{e}_u^k\|_{L^2} \end{aligned}$$

For the second term we can use the fact that $2\ \{\{w\}\}^2 \leq w_+^2 + w_-^2$, where w_+ and w_- are the restrictions of w on the two elements sharing F. The latter leads to

$$\sum_{F\in\mathcal{F}_h^I} 2\|\ \{\{w\}\}\ \|_{L^2}^2 \leq \sum_{\mathcal{K}\in\mathcal{T}_h} \|w\|_{L^2(\partial\mathcal{K})}^2$$

that we can use to estimate our second term. For the other ones we increase them by using the DG-norm and the $\boldsymbol{H}(\mathrm{div})$-norm.

$$\|e_\theta^k\|_{DG}^2 \leq \|\theta_h^k\|_{L^\infty}\frac{1}{C\sqrt{\nu_0}}\ \frac{5}{2}\ \|e_\theta^k\|_{DG}\|\sqrt{\nu_0}\ \boldsymbol{e}_u^k\|_{\boldsymbol{H}(\mathrm{div})} \tag{5.18}$$

We can simplify the DG-norm and then combine (5.18) with the first equation of (5.17).

$$\|\sqrt{\nu_0}\ \boldsymbol{e}_u^k\|_{\boldsymbol{H}(\mathrm{div})}\ +\ \|e_\theta^k\|_{DG} \leq \left(1 + \|\theta_h^k\|_{L^\infty} \frac{1}{C\sqrt{\nu_0}}\ \frac{5}{2}\right) \|\sqrt{\nu_0}\ \boldsymbol{e}_u^k\|_{\boldsymbol{H}(\mathrm{div})}$$

Let us call δ the constant that appears here. Now let us use $(5.17)_1$ to get

$$\|\sqrt{\nu_0}\ \boldsymbol{e}_u^k\|_{\boldsymbol{H}(\mathrm{div})}\ +\ \|e_\theta^k\|_{DG} \leq \delta\ \|\left(\nu(\theta_h^{k-1}) - \nu(\theta_h^k) + \beta|\boldsymbol{u}_h^{k-1}| - \beta|\boldsymbol{u}_h^k|\right)\ \boldsymbol{u}_h^k\sqrt{\nu_0}\|_{L^2}$$

Now we use the assumption that $\boldsymbol{u}_h^k \in [L^\infty(\Omega)]^2$, $\forall k$ which is physically possible since it is reasonable to assume that the velocity does not explode.

$$\|\sqrt{\nu_0}\ \boldsymbol{e}_u^k\|_{\boldsymbol{H}(\mathrm{div})}\ +\ \|e_\theta^k\|_{DG} \leq \delta\sqrt{\nu_0}\ \|\boldsymbol{u}_h^k\|_{L^\infty}\ \|\ \left(\nu(\theta_h^{k-1}) - \nu(\theta_h^k) + \beta|\boldsymbol{u}_h^{k-1}| - \beta|\boldsymbol{u}_h^k|\ \right)\|_{L^2}$$

Thanks to the Lipschitz property of $\nu(s)$ (we call L the Lipschitz constant) and the inverse triangular inequality for the Euclidean norm, we have

$$\|\sqrt{\nu_0}\ \boldsymbol{e}_u^k\|_{\boldsymbol{H}(\mathrm{div})}\ +\ \|e_\theta^k\|_{DG} \leq \delta\ \|\boldsymbol{u}_h^k\|_{L^\infty}\ \|L\left|\theta_h^{k-1} - \theta_h^k\right| + \beta\sqrt{\nu_0}\ \left|\boldsymbol{u}_h^{k-1} - \boldsymbol{u}_h^k\right|\ \|_{L^2}$$

By the triangular inequality for the L^2-norm in the right hand side we get,

$$\|\sqrt{\nu_0}\ \boldsymbol{e}_u^k\|_{\boldsymbol{H}(\mathrm{div})}\ +\ \|e_\theta^k\|_{DG} \leq \delta\ \|\boldsymbol{u}_h^k\|_{L^\infty}\ \|\ L\left|\theta_h^{k-1} - \theta_h^k\right|\|_{L^2} + \|\ \beta\sqrt{\nu_0}\ \left|\boldsymbol{u}_h^{k-1} - \boldsymbol{u}_h^k\right|\ \|_{L^2}$$

Finally,

$$\begin{aligned}\|\sqrt{\nu_0}\ \boldsymbol{e}_u^k\|_{\boldsymbol{H}(\mathrm{div})}\ +\ \|e_\theta^k\|_{DG} &\leq \delta\ \|\boldsymbol{u}_h^k\|_{L^\infty}\ \max\{L,\beta\}\left(\|e_\theta^{k-1}\|_{L^2} + \|\ \sqrt{\nu_0}\left|\boldsymbol{e}_u^{k-1}\right|\|_{L^2}\right)\\ &\leq \delta\ \|\boldsymbol{u}_h^k\|_{L^\infty}\ \max\{L,\beta\}\left(\|\sqrt{\nu_0}\ \boldsymbol{e}_u^{k-1}\|_{\boldsymbol{H}(\mathrm{div})}\ +\ \|e_\theta^{k-1}\|_{DG}\right)\end{aligned}$$

If $\delta\ \|\boldsymbol{u}_h^k\|_{L^\infty}\ \max\{L,\beta\}\ <\ 1$, then the scheme yields a contraction. We can iterate the scheme and since the constant is smaller than 1 we can deduce that the error between two consecutive iterations for velocity and temperature goes to zero if $k \to \infty$. For pressure we can consider the problem for errors (5.14) and exploit the inf-sup condition that holds (with a constant η) for the Darcy problem (see section 2.4) and say

$$\begin{aligned}\|e_p^k\|_{L^2(\Omega)} &\leq \frac{1}{\eta}\ \sup_{v_h\in V_h} \frac{\overset{k}{p}, \mathrm{div}\ \boldsymbol{v}_h)}{\|\boldsymbol{v}_h\|_{\boldsymbol{H}(\mathrm{div})}}\\ &= \frac{1}{\eta}\ \sup_{v_h\in V_h} \frac{(\nu(\theta_h^k) + \beta|\boldsymbol{u}_h^k|)\boldsymbol{e}_u^k, \boldsymbol{v}_h) - \left(\left(\nu(\theta_h^{k-1}) - \nu(\theta_h^k) + \beta|\boldsymbol{u}_h^{k-1}| - \beta|\boldsymbol{u}_h^k|\right)\ \boldsymbol{u}_h^k, \boldsymbol{v}_h\right)}{\|\boldsymbol{v}_h\|_{\boldsymbol{H}(\mathrm{div})}}\\ &\leq \frac{1}{\eta}\left(\left(\nu_1 + \frac{\beta}{\nu_0}M_u\right)\|\boldsymbol{e}_u^k\|_{L^2}\ +\ \frac{M_u}{\nu_0}\max\{L,\beta\}\left(\|\sqrt{\nu_0}\ \boldsymbol{e}_u^{k-1}\|_{\boldsymbol{H}(\mathrm{div})}\ +\ \|e_\theta^{k-1}\|_{DG}\right)\right)\end{aligned}$$

If velocity and pressure converge for $k \to \infty$ the pressure converges too, under the same assumptions as before. □

Remark: It is important to point out that the study of convergence for the algorithm has been carried out using the $\boldsymbol{H}(\mathrm{div})$-norm instead of the $\boldsymbol{X}$-norm, however since the $\boldsymbol{X}$-norm is stronger, the a-priori bound we found in proposition 3 holds the same for the $\boldsymbol{H}(\mathrm{div})$-norm.

5.3 Numerical experiment coupled problem

In this section we tested the iterative algorithm that solve the discrete form of the coupled problem. We considered a uniform conforming mesh $\mathcal{T}_h$ that discretize the domain $\Omega = (0,1)\times(0,1)$. We took inspiration by section **4.2**, therefore we fixed the tolerance to 1×10^{-8} and the maximum number of iterations to 40; moreover we defined a new metric to measure the error:

$$E = \frac{\|\boldsymbol{u}_h^k - \boldsymbol{u}_h^{k-1}\|_{\boldsymbol{H}(\mathrm{div};\Omega)}}{\|\boldsymbol{u}_h^k\|_{\boldsymbol{H}(\mathrm{div};\Omega)}} + \frac{\|p_h^k - p_h^{k-1}\|_{L^2(\Omega)}}{\|p_h^k\|_{L^2(\Omega)}} + \frac{\|\theta_h^k - \theta_h^{k-1}\|_{H^1(\Omega)}}{\|\theta_h^k\|_{H^1(\Omega)}}$$

then, at each iterations k, we solved a problem of type (5.12) in order to compute our approximation. With the same reasoning explained before, if the error is smaller or equal to the tolerance then the algorithm stops otherwise it goes on until the maximum number of iterations is reached. We used the following data for our numerical experiments:

$$\nu(\theta) = 1 + e^{-\theta}\,, \quad \kappa = 0.05\,, \quad \beta = 1.2\,, \quad g \equiv 0\,, \quad \boldsymbol{f} = \left[\nu(\theta_{ex}) + \beta\sqrt{2} + y\,,\, \nu(\theta_{ex}) + \beta\sqrt{2} + x\right]^T$$

with the exact solutions

$$\boldsymbol{u}_{ex} = [1,1]^T\,, \quad p_{ex} = xy\,, \quad \theta_{ex} = \frac{e^{\frac{x-1}{\kappa}} - e^{-\frac{1}{\kappa}}}{1 - e^{-\frac{1}{\kappa}}} + \frac{e^{\frac{y-1}{\kappa}} - e^{-\frac{1}{\kappa}}}{1 - e^{-\frac{1}{\kappa}}}$$

with boundary conditions that are inferred from the above exact solutions. We performed two tests, the first one with $r = 1$ (we recall that the parameter r control the degree of the discrete spaces, hence for $r = 1$ we have dG elements of order 1 and 0 for temperature and pressure respectively, instead elements of Raviart-Thomas of order 1 for the velocity) the second with $r = 2$. These are the results:

h	$\|\|\theta_{ex} - \theta_h\|\|_{L^2}$	$\|\|\boldsymbol{u}_{ex} - \boldsymbol{u}_h\|\|_{L^2}$	$\|\|p_{ex} - p_h\|\|_{L^2}$
$\frac{1}{8}$	4.676×10^{-2}	5.416×10^{-3}	1.708×10^{-2}
$\frac{1}{16}$	1.413×10^{-2}	1.533×10^{-3}	8.512×10^{-3}
$\frac{1}{32}$	3.721×10^{-3}	3.789×10^{-4}	4.253×10^{-3}
$\frac{1}{64}$	9.424×10^{-4}	9.424×10^{-5}	2.126×10^{-3}
$\frac{1}{128}$	2.378×10^{-4}	2.363×10^{-5}	1.063×10^{-3}

Table 5.1: $r = 1$

h	$\|\|\theta_{ex} - \theta_h\|\|_{L^2}$	$\|\|\boldsymbol{u}_{ex} - \boldsymbol{u}_h\|\|_{L^2}$	$\|\|p_{ex} - p_h\|\|_{L^2}$
$\frac{1}{8}$	6.093×10^{-3}	7.502×10^{-4}	2.750×10^{-4}
$\frac{1}{16}$	9.762×10^{-4}	1.099×10^{-4}	6.538×10^{-5}
$\frac{1}{32}$	1.361×10^{-4}	1.373×10^{-5}	1.627×10^{-5}
$\frac{1}{64}$	2.416×10^{-5}	1.979×10^{-6}	4.069×10^{-6}
$\frac{1}{128}$	7.123×10^{-6}	4.891×10^{-7}	1.017×10^{-6}

Table 5.2: $r = 2$

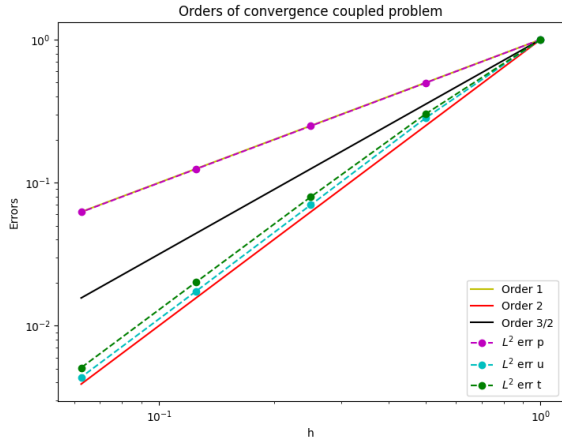

Figure 5.1: $r = 1$

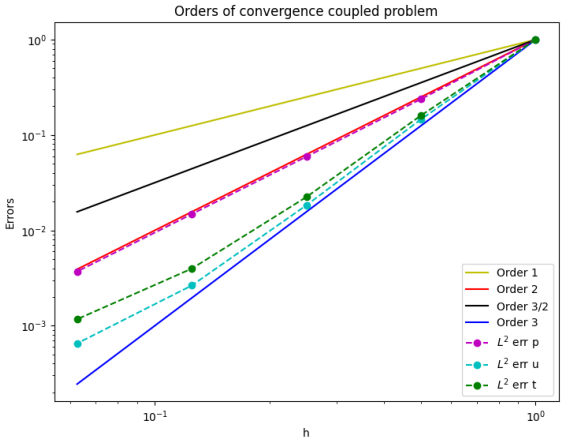

Figure 5.2: $r = 2$

In the first case (Fig. 5.1, Tab. 5.1) we obtained an order of convergence equal to one for the pressure and an order equal to two for both velocity and temperature. For pressure and temperature we observe the orders that we were expecting from theory. For velocity, despite that $\boldsymbol{u}_{ex} \in \boldsymbol{X}_h$, we do not observe the machine precision error since we are in the context of a linearization scheme, where non-linearities and couplings are "approximated". This yields to an order of convergence equal to two. These orders gave us confirmation of the good functioning of the iterative algorithm. In the second case (Fig. 5.2, Tab 5.2) we achieved an order equal two for the pressure and an order slightly greater than two for both temperature and velocity. The pressure presented the same behavior also for this experiment, namely a increment in the order by one. Also in this second case the velocity did not reach the machine precision, however its order of convergence increase by one. The temperature like the other unknowns improves its order by one, as we were expecting. For the details of the code we refer to the Python script named "STEP4-CoupledProblem".

Remark: In the plots all the errors are rescaled with respect to the first one of the corresponding series, while in the tables there are the absolute errors.

Conclusion

In this report we presented all the steps that led us to solve the Darcy-Forchheimer equation coupled with an advection-diffusion equation. After introducing the notations we separately analyzed the equations that build the complete problem, by presenting the respective weak and discrete formulations. For the advection-diffusion problem we proved skew-symmetry and coercivity of the discrete form. The problems were numerically tested individually and in cascade, in both cases the implementations showed robustness for advection dominant problems, moreover the results had validated the expected estimates. We tested the robustness of the iterative algorithm that resolved the non linearity in the Darcy-Forchheimer equation, namely we inspected its behavior whit different values of the parameter β. To conclude, we proved some a-priori bounds for the discrete version of the final coupled problem, moreover, we inspected the numerical behaviour of the iterative scheme that solved the coupled problem. The final goal of this project was to obtain some results for a discontinuous discretization of the Darcy-Forccheimer problem, which in literature is rarely treated with such numerical methods. This results could be useful as a reference for more in depth analysis and implementations, for example: (1) solve the same discrete problem over more complex geometries and meshes. (2) Using a dG approach also for the Darcy-Forccheimer problem in order to use non-conforming meshes. (3) Performing more in depth analysis for the complete coupled problem with more sophisticated techniques.

References

[1] G. Deugoue, J.K. Djoko, V.S. Konlack, M. Mbehou. *Numerical Analysis of a Darcy-Forchheimer Model Coupled with the heat Equations.* J. Sci. Comput., (2022) 92:55

[2] F. Brezzi, L. D. Marini. *Discontinuous Galerkin methods for First-Order Hyperbolic problems.* Math. Models Methods Appl. Sci., Vol. 14, No. 12 (2004) 1893-1903

[3] D. A. Di Pietro, A. Ern. *Mathematical Aspects of Discontinuous Galerkin Methods.* Springer (Berlin 2012)

[4] H. Pan, H. Rui. *Mixed Element Method for Two-Dimensional Darcy-Forchheimer Model.* J. Sci. Compit., (2012) 52:563-587

[5] A. Quarteroni. *Numerical Models for Differential Problems.* Springer, Volume 8, 5^{th} edition (Milano 2012)

[6] A. Quarteroni. Lecture notes of the course *Numerical Analysis for Partial Differential Equations*, Politecnico di Milano 2022/2023

[7] A. Cangiani, Z. Dong, E. H. Georgoulis, P. Houston. *Discontinuous Galerkin Methods on Polygonal and Polyhedral Meshes.* Springer (2017)

[8] Y. Achdou, C. Bernardi, F. Coquel. *A priori and a posteriori analysis of finite volume discretizations of Darcy's equations.* Numer. Math. (2003) 96: 17-42